

# Large-scale orientational order in bacterial colonies during inward growth

## Authors

Mustafa Basaran<sup>1,2\*</sup>, Y. Ilker Yaman<sup>1\*</sup>, Tevfik Can Yüce<sup>1</sup>, Roman Vetter<sup>3,4</sup> and Askin Kocabas<sup>1,2,5,6†</sup>

<sup>1</sup>Department of Physics, Koç University, Sarıyer, Istanbul, Turkey 34450

<sup>2</sup>Bio-Medical Sciences and Engineering Program, Koç University, Sarıyer, Istanbul, Turkey 34450

<sup>3</sup>Computational Physics for Engineering Materials, ETH Zurich, 8093 Zurich, Switzerland

<sup>4</sup>Current address: Department of Biosystems Science and Engineering, ETH Zurich, 4058 Basel, Switzerland

<sup>5</sup>Koç University Surface Science and Technology Center, Koç University, Sarıyer, Istanbul, Turkey 34450

<sup>6</sup>Koç University Research Center for Translational Medicine, Koç University, Sarıyer, Istanbul, Turkey 34450

\*These authors contributed equally.

†Corresponding author: [akocabas@ku.edu.tr](mailto:akocabas@ku.edu.tr)

## **Abstract**

During colony growth, complex interactions regulate the bacterial orientation, leading to the formation of large-scale ordered structures, including topological defects, microdomains, and branches. These structures may benefit bacterial strains, providing invasive advantages during colonization. Active matter dynamics of growing colonies drives the emergence of these ordered structures. However, additional biomechanical factors also play a significant role during this process. Here we show that the velocity profile of growing colonies creates strong radial orientation during inward growth when crowded populations invade a closed area. During this process, growth geometry sets virtual confinement and dictates the velocity profile. Herein, flow-induced alignment and torque balance on the rod-shaped bacteria result in a new stable orientational equilibrium in the radial direction. Our analysis revealed that the dynamics of these radially oriented structures also known as aster defects, depend on bacterial length and can promote the survival of the longest bacteria around localized nutritional hot spots. The present results indicate a new mechanism underlying structural order and provide mechanistic insights into the dynamics of bacterial growth on complex surfaces.

## **INTRODUCTION**

Bacterial colonization and invasion are collective phenomena. These processes are regulated through a complex interplay of physical and biological interactions in a crowded population. Bacterial morphology, hydrodynamics, surface topology, and topography markedly alter growth mechanisms, morphology, and overall competition among bacteria[1-6]. Elucidation of the factors regulating collective bacterial growth and their competition is essential to enhance our

understanding of evolutionary dynamics, bacterial infection, and the progression of inflammatory diseases.

A characteristic feature of bacterial colonization is the formation of large-scale order. Rod-shaped bacteria display nematic alignment on surfaces, wherein localized stress, surface friction, and elasticity trigger the formation of ordered domains and lead to the emergence of topological defects[7-11] and various types of self-assembled structures, including edge fingerings[12] and vertical structures[13, 14].

In particular,  $\pm \frac{1}{2}$  topological defects are the typical orientational singularities observed among growing bacterial colonies and biofilms[7, 9, 10, 15]. These topological defects have biological significance and regulate stress distribution across the structure, alter the physiology of the cells[16], and could control entire morphology; eventually, these effects trigger the formation of fruiting bodies[17] and bacterial spores in biofilms[15]. Liquid crystal theory has successfully predicted the dynamics of these defects;  $-\frac{1}{2}$  defects are stationary whereas  $+\frac{1}{2}$  defects are generally motile[18-20]. Another interesting structural order in bacterial colonies is anchoring, where the bacteria are tangentially oriented along the edge of the colony[2, 7, 8].

In this study, we assess the orientational dynamics of a crowded bacterial population competing for limited space. Unlike regular expanding colonies, if growing bacteria surround a closed area, domains of inward growth are formed. Under these conditions, entire mechanical interactions differ and lead to the formation of asters, formed as radially aligned +1 topological defects. With only a few exemptions[21, 22], higher-order topological defects[23, 24] are not commonly observed in extensile active matter systems, including growing bacterial colonies. These defects only appear under external modifications such as stress[25], confinement[26, 27], and flow[28].

Our results also reveal that velocity profile is an important factor controlling the emergence of these radially aligned structures. Furthermore, we investigate the invasive advantages of this orientation for competing bacterial strains of different lengths.

Inward growth is commonly observed in various biological systems. During wound healing[29], cancer cell growth[30, 31], and retina development[32, 33], similar dynamic mechanisms are underway. Our results may provide novel mechanistic insights into these dynamics, particularly on the physical conditions for radial structural alignments during these complex growth processes.

## RESULTS

### Experimental observation of aster structures

To observe the dynamics of inward-growing bacterial colonies, we sparsely spread nonmotile *Escherichia coli* and *Bacillus subtilis* separately, on a flat agarose surface (see Materials and Methods). Time-lapse fluorescence microscopy was then performed to investigate the temporal evolution of growing colonies. With colony growth, the closed area invaded by multiple colonies was observed across the plate. Rough colony interfaces gradually converge to symmetric, relatively smooth, and enclosed circular areas. We refer to these shrinking circular regions as inward-growing bacterial domains because the growth direction is towards the center of the area. Figure 1 displays typical snapshots of the inward growth process (Fig. 1a, b, Video 1, (Figure 1—video 1)). Unlike regular expanding colonies, the bacterial orientation around these domains is generally radial. To assess the orientation, we first analyzed the radial order parameter  $S_R$  around

the center of these domains. The radial order parameter  $S_R$  can be expressed as:

$$\langle S_R \rangle = \frac{1}{N} \sum_i \cos [2(\theta^i - \phi^i)] \quad (1)$$

where  $\theta^i$  is the angular orientation with respect to x-axis and  $\phi^i$  is the angular position of the bacterium  $i$  in polar coordinates about the colony center. Figure 1 d and c display the bacterial orientation and order parameter  $S_R(r)$  as a function of radial distance.  $S_R = +1$  corresponds to radial alignment and  $S_R = -1$  corresponds to tangential alignment. It is evident that large-scale radial order emerges across these inward growing domains (Fig. 1c, d). These structures strongly resemble +1 topological defects also known as aster structures. We also measured the velocity of the bacterial flow during this process (Fig. 1d). We found that the direction of the flow is towards the center. From these measurements, we can conclude this radial inward flow could align the bacteria in a radial direction.

### **Numerical simulation of bacterial orientation during inward growth**

To clarify the impact of flow-induced alignment and differences in orientation between inward-growing and regular expanding colonies, we simulated 2D bacterial growth using a hard rod model. We used the open-source simulation code GRO [34] which provides a fast platform to observe bacterial growth (see Materials and Methods). To determine the morphology of the inward growing domain, we initially distributed bacteria in a random orientation. With growth, bacteria form small colonies, which eventually fuse into a growing annulus (Fig. 1e). To visualize the large-scale order, we color-coded bacteria on the basis of their radial orientation, with red representing radial orientation, and blue representing tangential orientation around the

center of the hole (Fig. 1e, Video 2). These simulation results captured the experimentally observed radial order across the colony.

However, regular expanding colonies only formed microdomains with random local orientations (Fig. 1g, Figure 1-video 2). Regular expanding colonies represent the outward growth initiating from a single bacterium displayed in Figure 1g. Based on these simulations, the primary difference between regular expanding and inward-growing colonies is the sudden change in the direction of the surface drag force which depends on the velocity (Fig. 1f, h). In inward-growing colonies, this force flips its sign at a critical radius where the local radial velocity of the colony vanishes.

To further quantify the effects of the critical radius, we determined the stress distribution and radial velocity profile  $v_r$ , in growing colonies. Figure 2 summarizes the comparison and time evolution of these parameters. We first focused on radial and azimuthal stress profiles. We noted that the stresses ( $|\sigma_{rr}|$  and  $|\sigma_{\theta\theta}|$ ) (Figure 2—figure supplement 1) are maximum around the critical radius during inward growth (Fig. 2a, b). The stress profiles initially show the quadratic form which is particularly dictated by the radial velocity profile[13].

Then we observed that, as colonies grew, only inward-growing colonies developed substantial radial order  $S_R(r)$  (Fig. 2c, d). Furthermore, radial velocity profiles  $v_r$  significantly differed between regular expanding and inward-growing colonies. In contrast with regular expanding colonies, which have a linear radial velocity profile, inward-growing colonies developed radially nonlinear velocity, which vanishes at the critical radius (Fig. 2e, f, Figure 2—figure supplement 3). Experimentally, similar profiles were measured (Figure 2—figure supplement 4). This profile gradually rotated the bacteria into the radial direction (Fig. 2g, Figure 2—figure supplement 5). Based on these results, the velocity profile appears to be the key physical parameter regulating

the flow-induced alignment and the formation of the radial order.

### **Velocity profile and radial alignment**

To better understand the association between the velocity profile on radial alignment, we first focused on the development of a minimum theoretical model based on active nematics. The theory of active nematics and liquid crystal physics provides a robust framework for understanding the dynamics of bacterial orientation. The primary characteristic of expanding colonies is the constant growth rate of the colony structure. The incompressibility criteria in 2D results in a linear relation between bacterial growth rate and radial velocity profile of the colony,  $v_r = g(r)r = \frac{\Lambda}{2}r$ , where  $g(r)$  is the local growth rate and  $\Lambda$  is the exponential bacterial growth rate. These coefficients are related to incompressible expanding bacterial colonies.

This relation was previously referred to as a Hubble-like constant owing to its similarity to the expansion of the universe[8]. We considered the same approximations to obtain insights into bacterial orientation during inward growth. First, we used the assumption that without molecular field and convection terms, the time evolution of the orientational angle  $\theta$  is simply regulated as follows (see Materials and Methods):

$$\frac{d\theta}{dt} = \frac{\xi g' r}{2S} \sin(2(\phi - \theta)) \quad (2)$$

where  $\phi$  is the angular position of the bacteria in polar coordinates, and  $\xi$  is the flow alignment parameter. Furthermore,  $g(r)$  is the local growth rate of the colony and its spatial derivative  $g'(r)$  regulating the stability of the bacterial orientation. The constant growth rate observed in regular expanding colonies does not provide any orientational preference,  $\frac{d\theta}{dt} = 0$ . However, this

condition significantly differs during inward growth, wherein the local growth rate can be expressed as follows:

$$g(r) = \frac{v_r}{r} = \frac{\Lambda (r^2 - R_c^2)}{2 r^2} \text{ and } g'(r) = \Lambda \frac{R_c^2}{r^3} > 0 \quad (3)$$

Our assumption of a constant critical radius (Supplementary Fig. 1b) indicates that the spatial derivative of the growth rate is positive everywhere across the colony,  $g'(r) > 0$ , suggesting the possibility of a stable state with  $\theta = \phi$ . The stable radial orientation stimulates aster formation, being referred to as a +1 topological defect. This finding is significant because  $g'(r) \neq 0$  is generally possible in compressible structures and also only around leading edges of growing colonies due to sudden drop[8]. Although bacterial colonies are not compressible, inward growth and the shrinking hole structure alter the overall velocity profile and lead to an essential local growth rate.

The radial orientation is stable throughout the colony and not only below the critical radius. To clarify this point, we simulated colony growth under a fixed circular wall mimicking the stationary critical radius (Figure 2—figure supplement 6). We observed a similar radial alignment. These results indicate the association between the circular confinement owing to the critical radius which dictates velocity profiles and the stability of bacterial orientations.

### **Nemato-hydrodynamics and continuum modeling**

Thereafter, we investigated whether the same defects were obtained through the continuum nemato-hydrodynamics equations of growing active matter[35-37]. Due to coarse graining over specific physical details, the continuum model could provide generality of our observation. The model is based on continuity, Navier–Stokes equations, and dynamics of the



order parameter tensor  $\mathbf{Q}$ (see Materials and Methods). The coupled differential equations governing the primary material fields density  $\rho$ ,  $\mathbf{Q}$ , and velocity  $\mathbf{v}$  can be expressed as follows:

$$\frac{D\rho}{Dt} = \Lambda\rho + D_\rho\nabla^2\rho \quad (4)$$

$$\frac{D(\rho\mathbf{v})}{Dt} = \nabla \cdot \boldsymbol{\sigma} - \gamma\rho\mathbf{v} \quad (5)$$

$$\frac{D\mathbf{Q}}{Dt} = \xi\mathbf{u} + \mathbf{Q} \cdot \boldsymbol{\omega} - \boldsymbol{\omega} \cdot \mathbf{Q} + \Gamma^{-1}\mathbf{H} \quad (6)$$

Here,  $\frac{D}{Dt}$  is the material derivative, and the stress tensor is given as

$$\boldsymbol{\sigma} = -p\mathbf{I} - a(\rho)\mathbf{Q} - \xi\mathbf{H} + \mathbf{Q} \cdot \mathbf{H} - \mathbf{H} \cdot \mathbf{Q} \quad (7)$$

Here,  $a(\rho)\mathbf{Q}$  represents the active stress originating from the extensile nature of bacterial growth.  $\mathbf{u}$  and  $\boldsymbol{\omega}$  are the traceless strain rate and vorticity, respectively (see Materials and Methods). The critical parameter  $\xi$  is the flow alignment parameter. The details of the frictional drag coefficient per unit density  $\gamma$ , the molecular field  $\mathbf{H}$ , pressure  $p$ , rotational diffusion constant  $\Gamma$ , and small diffusion coefficient  $D_\rho$  are given in Material and Methods. These equations were initially solved for growing bacterial colonies[3, 7, 8, 10, 38] and successfully predicted the active nematic nature and domain formations among colonies of rod-shaped bacteria. We solved them numerically with finite element method (FEM) (see Materials and Methods). As a benchmark, we compared the simulations with regular expanding colonies. Figure 3 summarizes the results of these continuum simulations. As expected, regular expanding colonies exhibited only local alignment (Fig. 3a, c, Figure 3-video 1) corresponding to microdomains. However, inward-growing colonies developed robust radial alignment and order not only below but also beyond the critical radius (Fig. 3b, d, Video 3). Inward-growing colonies also displayed the expected nonlinear velocity profile required for radial alignment (Fig. 3e, f , Figure 3-video 2, 3, Figure 3- figure supplement 1). Moreover, a sudden drop of the velocity

profile near the inner and outer colony edges also resulted in tangential orientation. These results from continuum simulation suggest that similar radial alignment could be also observed in other active matter systems under the same radial velocity profiles.

### **Inward growing domains in multi-layered colonies**

Growing bacterial colonies on elastic substrates generally form multi-layered structures. We investigated whether these multilayered structures could change the radial alignment during inward growth. Herein, experimentally we observed inward growing domains only around the inner edge surrounded by dense multi-layered structures. This is because merging colonies and the accumulated stress trigger multi-layer formation and limit the size of monolayer region around the edge (Figure 4—figure supplement 1). We investigated whether these multilayered structures affect the radial alignment during inward growth by performing three-dimensional FEM simulations based on recently developed algorithms[15, 39, 40]. Our previous computational tool (GRO) cannot simulate bacterial growth in 3D. Our FEM algorithms are relatively slow, but this approach is very powerful to capture detailed bacterial growth in 3dimensional complex environments. The bacterial cells were modeled as growing elastic rods that undergo controlled cell division during colony growth. We first tested the 3D capability of FEM simulations by replicating similar radial alignment under spherical confinement (Figure 4—figure supplement 2). Then we focused on growing colonies on flat surfaces with surface friction. Figure 4 shows the prototypical FEM simulation outcome from inward-growing colonies. As expected, accumulated stress triggers verticalization and multi-layer formation around the critical radius of the colony (Fig. 4a, b and Video 4). However, a bacterial monolayer was observed only around the inner and outer leading edges of the

colony. The formation of a monolayer region around growing colonies has been investigated in great detail[4]. We found that these monolayers could also result in planar radial alignment (Video 5). The width of the monolayer was approximately  $\Delta r = 90 \pm 30 \mu m$  (Fig. 4c). This width defines the size of the aster structures observed herein.

### **Inward growing domains in monolayer colonies**

So far, we experimentally studied naturally emerged inward growing domains on agar surfaces. These domains are randomly formed across the plate. Due to random seeding of bacteria, outward growing edges of multiple colonies merge and form multilayered structures. In these experiments particularly, the confinement is defined by crowded multilayered environments. Thus, observing critical radius, outer growing edge and detailed velocity profiles are not possible around these dense regions. Our simulations showed that the initial annulus shape could overcome these limitations. We asked whether we could induce similar annulus structures by patterning the initial distribution of bacteria to observe both inward and outward growing domains. We first tried to imprint bacteria on an agarose surface using soft PDMS molds. However, the wet surface and capillary effect quickly disturbed the initial bacterial patterns defined by the mold. Then we preferred non-contact lithographic techniques for patterning. Using a photomask (Figure 5—figure supplement 1), we exposed randomly distributed bacteria with blue light to define an initial growth geometry by killing the remaining part of the pattern (see Materials and Methods). Figure 5a shows the time evolution of growing bacteria starting from annulus-shaped initial distribution. We observed that on a regular agar surface, again multi-layer formation dominates the overall colony morphology. Only

very narrow monolayer regions are observable around the inner and outer edges of the colony. We then focus our attention on how to eliminate this multilayering process. A simple glass or PDMS confinement cannot eliminate this multi-layering (Figure 4—figure supplement 1). Previous studies showed that attractive biochemical interactions between bacteria and surface could generate additional strong friction force[41]. Altogether friction force, stress accumulation, and verticalization of bacteria in a monolayer colony trigger the formation of these multi-layered structures. This process is mainly controlled by the competition between vertical force and lateral compression in the colony[1, 13, 41, 42]. Above the critical stress level, the orientation of rod-shaped bacteria becomes unstable and triggers the extrusion. Performing FEM simulations, we noticed that this extrusion process occurs around the center of the annuli and it can be controlled by surface friction (Figure 5- figure supplement 2). Although we don't know the detailed biological mechanism behind the friction force it is evident that minimizing the surface friction can increase the size of the monolayer colony. Then, we tested the same bacterial patterning on different membranes to find a surface with low friction by minimizing biochemical interaction. We noted that only polycarbonate (PC) surfaces are useful for this purpose, and they support large monolayer colonies while providing a sufficient bacterial growth rate (Figure 5—figure supplement 3, Figure 5-video 1, see Materials and Methods). The size of these monolayer colonies was approximately 600  $\mu\text{m}$ . As we observed in our previous simulations (Figure 4), at a later stage, the second layer formation appeared around the center of these annulus shapes which is close to the critical radius (Figure 5a, Figure 5-video 2). Similarly, we observed strong radial alignment across the colony (Figure 5c, d, Figure 5—figure supplement 4, 5). We did not observe any radial alignment in regular isolated monolayer colonies. Instead, we clearly observed orientational defects and microdomains in these monolayer colonies on PC surfaces

(Figure 5—figure supplement 6). Inward and outward growing monolayer domains also provided the nonlinear velocity profile (Figure 5e), which is essential for radial alignment. We noticed that during this process critical radius shows a constant profile (Figure 5f, Figure 5—figure supplement 7, Figure 5-video 2). The other interesting form of bacterial growth is biofilm formation which has filamentous and nematic internal structures. As a next step, we similarly tested the radial alignment dynamics of these bacterial biofilms during the inward growth process, starting from the same initial distribution. We used a biofilm-forming strain *B. Subtilis* 168[15] and observed similar strong radial alignment across the biofilms (Figure 5-video 3, Figure 5—figure supplement 8). Our FEM simulations also captured the alignment process of growing elastic bacterial biofilm structures (Figure 5-video 4, Figure 5—figure supplement 8 c, d).

### **Biological significance**

Finally, to assess the biological significance of radial alignment, we investigated whether these structures potentially affect the competition among bacteria during inward growth. In general, near the leading edge of a bacterial colony, competition strongly depends on physical parameters. The most prominent example is a genetic drift based on random fluctuations[43, 44]. This phenomenon could be altered through steric interactions among the cells, which can potentially alter the evolutionary dynamics of competing bacteria[45]. Although bacterial orientation is generally tangential at the expanding colony edge, radial bacterial alignment potentially contributes to inward growth. We hypothesized that longer rod-shaped bacteria

potentially have an advantage owing to the torque balance. The basic premise is that the torque depends on the length of the bacteria, resulting in rapid radial alignment. Radial alignment further leads to lane formation and promotes an invasive advantage to the longest one, which could be beneficial in terms of approaching nutritional hotspots localized around the defect core more effectively.

To assess this competition, we initially simulated the growth dynamics of a mixed population with different division lengths from the same random initial distribution on a circle (Figure 6—figure supplement 1). This is the most challenging condition to test the impact of the length difference on the bacterial alignment. Although the initial distribution of the bacteria is random, long bacteria can develop a higher radial order during inward growth (Fig. 6a-f). This radial order gradually allows the longest bacteria to approach the center of the defect more effectively (Fig. 6g). The bacterial growth is local, and it can create strong segregation within the colonies. The impact of the length could be more significant in segregated colonies. To visualize the difference, we initially segregated the bacterial strains with different lengths around the edge of the colony. Similar segregation can be commonly observed around the edge of the colony owing to random fluctuations. These segregations can also occur during inward growth (Figure 6—figure supplement 2). Instead of expanding segments owing to perimeter inflation, we observed shrinking segments owing to the deflation of the hole geometry. Computationally, the advantage of radial alignment was more evident in segregated bacterial colonies (Fig. 6h). Interestingly, in a monolayer colony, radial alignment promotes the invasion of both the center and the leading outer edge of the colony through the longest bacteria (Fig. 6g). After the complete invasion of the center, the radial lanes buckle (Figure 6—figure supplement 3, Video 6, 7). However, experimental verification of this competition

remains challenging. Although precise regulation of the aspect ratio of bacterial morphology is well established[46], cell length can still not be independently tuned without perturbing other essential physiological properties, including growth rate and the biofilm-forming potential of the bacteria.

## Discussion

Radially aligned structures can be considered as a +1 aster defect. These are ubiquitous topological structures observed in biological[47-50] or synthetic[51, 52] active matter systems. For instance, microtubules can form nematic alignment or asters during mitosis, depending on the extensile or contractile activity. Bacterial colonies can be considered an extensile active material platform, generally supporting the formation of only  $\pm \frac{1}{2}$  topological defects. This study shows that stable radially aligned, aster structures can also emerge during inward growth. In particular, we report the critical role of the colony velocity profile during this process, which depends on numerous factors. Although the bacterial growth rate is constant throughout the colony, growth geometry, confinement, or boundary conditions can alter the velocity profile. Together, these biomechanical interactions change the bacterial orientation and stability, thus generating ordered structures. Different types of ordered structures have been observed in bacterial biofilms[53] and 3D colonies[4]. Furthermore, we believe that the velocity profile of growing structures on flat surfaces plays a significant role in bacterial alignment. Future studies are required to investigate the contribution of these effects.

We should emphasize that inward growing bacterial colonies and wrinkling thin circular sheets have geometric similarities[54]. In these elastic circular objects, under axisymmetric tensile load, azimuthal stress (hoop stress,  $\sigma_{\theta\theta}$ ) show transition from tensile to compressive profile which

eventually creates radial wrinkling pattern below critical radius. However, unlike elastic objects, growing bacterial colonies can only develop compressive stress due to negligible attractive force between bacteria. Experimental measurement of internal stress could provide more details, but it remains challenging. We noticed that the packing fraction of the bacteria shows a correlated profile (Figure 2—figure supplement 2). However, particularly for aligned bacteria, it is still very difficult to extract this information. In the future, new molecular probes could be useful for the experimental measurement of accumulated stress in the bacterial colonies[55, 56].

Finally, this study reveals the potential biological significance of radial alignment during the invasion. These ordered structures provide additional advantages and promote the survival of the longest bacteria. These results link the orientational properties and competition dynamics of bacterial colonies. Our findings are of potential relevance for the understanding of complex dynamics of bacterial infections and the progression of inflammatory diseases.

## **Materials and Methods**

**Bacterial preparation and growth conditions.** Bacterial cultures (BAK47 and BAK51) were grown in Luria-Bertani (LB) broth at 37 °C on a shaker. An overnight culture was diluted 100x and grown for 8 h. The culture was diluted 10000x, and 10 µl of culture was seeded on an LB agarose plate. These isolated bacteria on plates were grown at 21 °C for 12 h and then imaged. Strains used in experiments are described in Table 1. In *B. Subtilis* bacterial strains, the flagella-producing gene (*hag*) was mutated to eliminate the swimming-induced motion. The background strain TMN1138 was obtained from R. Losick Lab.



**Microscopy imaging.** Fluorescence time-lapse imaging was performed using a Nikon inverted and Stereo SMZ18 microscopes. Images were obtained using a Andor EMCCD camera. Time intervals between successive images were set to 5-10 minutes.

**2D hard-rod simulations of a growing colony.** We used the open-source simulation program GRO based on a hard-rod model. The code is available from <https://depts.washington.edu/soslab/gro/>. We modified the original code to be able to change the initial bacterial position and to extract the orientation of the bacteria.

### **Bacterial patterning.**

We used photolithographic techniques to define the initial distribution of the bacteria by killing with structured blue light illumination. We used 15 min exposure under  $5\text{mW/mm}^2$  480 nm uniform light beam. We think the killing mechanism is mainly based on the local drying process. The geometry was defined by chromium photomask. The mask (**Supplementary Fig. 8**) was fabricated by using Heidelberg DWL 66+ Direct Writing Lithography System and developed with chromium etchant. We have tested different annulus-shaped patterns by tuning the inner and outer radius. Due to light diffraction, the final exposed pattern depends on the spacing between the PC filter and a mask. Our optimized pattern has 400  $\mu\text{m}$  inner and 800  $\mu\text{m}$  outer radius.

### **Growing monolayer colonies on low friction surfaces.**

In order to minimize surface friction, we replaced the agarose surface with a filter membrane. We have tested several membrane filters, including nylon, polycarbonate (PC), polyethersulfone, cellulose acetate. Only white PC filters with 0.4  $\mu\text{m}$  pore size supported stable and large-scale monolayer colony formation. We noted that the brown PC filter has similar low surface friction;

however, it has strong light absorption and does not allow noncontact lithography due to heavy condensation on the photomask.

**SEM imaging.** A PC filter paper with a pore size of 0.4  $\mu\text{m}$  was placed on LB agar surface. After seeding the 10000x diluted bacteria on the filter paper, bacteria were grown on the paper for 12 h at 21  $^{\circ}\text{C}$ . Then the filter paper was peeled off from the surface, and the colonies were fixed using paraformaldehyde and left to dry. Fixed colonies were coated with 20nm gold and imaged using a Zeiss Ultra Plus Field Emission Electron Microscope.

### Calculating stress distribution in a growing colony

The stress inside the colony can be calculated from the virial expansion [3]  $\sigma_i = \frac{1}{2a'_i} \sum_j r_{ij} F_{ij}$ ,  $a'_i$  is the effective area,  $r_{ij}$  is the position of the contact and  $F_{ij}$  is the interaction force between the cells. Using the following transformations, we calculated the stress in polar coordinate

$$\sigma_{rr} = \sigma_{xx} * \cos^2(\theta) + \sigma_{yy} * \sin^2(\theta) + \sigma_{xy} * \sin(\theta) * \cos(\theta)$$

$$\sigma_{\theta\theta} = \sigma_{xx} * \sin^2(\theta) + \sigma_{yy} * \cos^2(\theta) + \sigma_{xy} * \sin(\theta) * \cos(\theta)$$

$$\sigma_{\theta r} = \cos(\theta)\sin(\theta)(\sigma_{yy} - \sigma_{xx}) + \sigma_{xy} * \cos(2 * \theta)$$

Due to negligible lateral friction between bacteria, we ignore  $\sigma_{xy}$  and our equations become:

$$\sigma_{rr} = \sigma_{xx} * \cos^2(\theta) + \sigma_{yy} * \sin^2(\theta)$$

$$\sigma_{\theta\theta} = \sigma_{xx} * \sin^2(\theta) + \sigma_{yy} * \cos^2(\theta)$$

$$\sigma_{\theta r} = \cos(\theta)\sin(\theta)(\sigma_{yy} - \sigma_{xx})$$

**3D FEM simulations of growing bacterial colonies.** For the 3D computer simulations, we employed an open-source (<https://libmesh.github.io/>) parallel finite element library written in C++[40]. Analogous to[15], the bacteria were modeled as an isotropic, linearly elastic continuum whose initial stress-free shapes were spherocylinders. The bacteria were assumed to maintain a uniform circular cross-section with radius  $r = 0.5\mu\text{m}$ , a mass density of  $1\text{gcm}^{-3}$ , a Young's modulus of  $E = 5300\text{Pa}$ , and a Poisson ratio of  $\nu = 1/3$ . The total elastic energy  $U$  of each bacterium comprised the usual terms for axial dilatation or compression, bending, and torsion[39]:

$$U = \frac{E\pi r^2}{2} \int_0^L \varepsilon^2 + \frac{r^2}{4} \left( \kappa^2 + \frac{1}{1+\nu} \varphi^2 \right) ds$$

where  $L$  denotes the bacterium length,  $\varepsilon$  the axial Cauchy strain,  $\kappa$  the scalar midline curvature, and  $\varphi$  the twist per unit length. Hertzian steric forces were exchanged between overlapping bacterial elements in a normal direction. Tangential forces and torques exchanged during contact between bacterium pairs and between bacteria and the substrate was computed with a slip-stick friction model with a uniform isotropic Coulomb friction coefficient. We modeled the substrate as an elastic half-space onto which the bacterial colony was placed, and exerted a perpendicular gravitational force on the bacteria. The bacteria were grown exponentially in length over time by continuously increasing each element's equilibrium length. For this study, the finite element program was extended to allow for cell division when the bacterial length surpassed a division threshold  $L_\theta = 5\mu\text{m}$ . When  $L > L_\theta$ , the bacteria were split into two pieces at a random position drawn from a normal distribution about their center with a standard deviation of  $L/10$ , but no further away from the center than  $L/5$ . To evolve the colony in time, Newton's translational and

rotational equations of motion were integrated with a Newmark predictor-corrector method of second order. To equilibrate the colony during growth, viscous damping forces were added.

In order to simulate inward growing biofilm structure, we used our previous biofilm model[15] and the same parameters. 8 identical replica of small biofilm structures are circularly distributed to form an initial annulus shape. We used fracture strain (0.3) to relax the extreme bending condition by triggering filament division.

### Radial Velocity Profile.

To calculate radial velocity profile,  $v_r$ , during inward growth, we assume there is a critical radius  $R_c$ , where  $v_r$  is equal to zero. For  $r < R_c$  and the initial domain size equals to  $A_{in}$ :

$$A(t) = A_{in}e^{\Lambda t} = \pi(R_c^2 - r^2) \quad (8)$$

If we take derivative wrt. time.

$$A_{in}\Lambda e^{\Lambda t} = -2\pi r \frac{dr}{dt} \quad (9)$$

$$v_r(r, t) = \frac{dr}{dt} = -\frac{\Lambda A(t)}{2\pi r} = \frac{\Lambda(r^2 - R_c^2)}{2r} \quad (10)$$

For outer growth where  $r > R_c$

$$A(t) = A_{out}e^{\Lambda t} = \pi(r^2 - R_c^2) \quad (11)$$

Similarly, the time derivative is

$$A_{out}\Lambda e^{\Lambda t} = 2\pi r \frac{dr}{dt} \quad (12)$$

$$v_r(r, t) = \frac{dr}{dt} = \frac{\Lambda A(t)}{2\pi r} = \frac{\Lambda(r^2 - R_c^2)}{2r} \quad (13)$$

Which results in the same equation. Consider that for  $r$  lower than  $R_c$ , velocity will be negative (inward direction) and for  $r$  greater than  $R_c$  velocity will be positive (outward direction).

**Continuum Modeling.** For the continuum modeling, Eq.4-7 were solved with the finite element method (FEM) in COMSOL Multiphysics. The material derivative is given by  $D/Dt = \partial_t + \mathbf{v} \cdot \nabla + (\nabla \cdot \mathbf{v})$ .  $\mathbf{u}$  and  $\boldsymbol{\omega}$  are the strain rate and vorticity tensors, respectively, with components  $u_{ij} = (\partial_i v_j + \partial_j v_i - \delta_{ij} \nabla \cdot \mathbf{v})/2$  and  $\omega_{ij} = (\partial_i v_j - \partial_j v_i)/2$ . We constructed a traceless and symmetric Q-tensor field:

$$Q_{\alpha\beta} = S \left( n_\alpha n_\beta - \frac{1}{2} \delta_{\alpha\beta} \right) \quad (14)$$

and we defined scalar order parameter:

$$S(r) = 2 \sqrt{Q_{xx}^2(r) + Q_{xy}^2(r)} \quad (15)$$

The molecular field  $\mathbf{H}$  can be obtained starting from the Landau-de Gennes free energy density given as:

$$f_{LdG} = \frac{1}{2} K |\nabla \mathbf{Q}|^2 + \frac{1}{2} \alpha(\rho) \text{tr}[\mathbf{Q}^2] + \frac{1}{4} \beta(\rho) (\text{tr}[\mathbf{Q}^2])^2 \quad (16)$$

Therefore  $\mathbf{H} = \delta/\delta \mathbf{Q} \int dA f_{LdG} = K \nabla^2 \mathbf{Q} - \alpha(\rho) \mathbf{Q} - \beta(\rho) \text{tr}[\mathbf{Q}^2] \mathbf{Q}$ . In the simulations, the relationships  $a(\rho) = a_0 \rho$ ,  $\beta(\rho) = \frac{\alpha_0}{2} \rho$ ,  $\alpha(\rho) = \alpha_0 (\rho_c - \rho)$  and  $p = G * \max \left\{ \left( \frac{\rho}{\rho_0} - 1 \right), 0 \right\}$  were used. We set the initial cell density  $\rho_0 = 1$ , growth rate  $\Lambda = 0.005$ , frictional drag coefficient per unit density  $\gamma = 0.2$ , flow aligning parameter  $\xi = 0.7$ , rotational diffusion constant  $\Gamma = 1$ , and the remaining parameters  $a_0 = 0.002$ ,  $\alpha_0 = 0.01$ ,  $\rho_c = \rho_0/2 = 0.5$ ,  $G = 2$ ,  $D_\rho = 0.04$ ,  $K = 0.01$ .

**Approximation for growth-induced alignment.** The following approximation and equations are received from Dell'Arciprete et.all [8]. These approximations were used to explain the

tangential alignment of bacteria at the edge of growing colonies. The equation of motion for 2D nematodynamics without any free energy and no spatial variation of  $Q$  can be written as

$$\frac{\partial Q_{\alpha\beta}}{\partial t} + v_\gamma \partial_\gamma Q_{\alpha\beta} = \xi u_{\alpha\beta} - Q_{\alpha\gamma} \omega_{\gamma\beta} + \omega_{\alpha\gamma} Q_{\gamma\beta} \quad (17)$$

If we assume

$$v_r = g(r)r \quad (18)$$

From this formulation we can conclude that :

$$v_\alpha = g(r)x_\alpha \quad (19)$$

Where  $x_\alpha$  is the Cartesian component of the position vector

$$\partial_\beta v_\alpha = g \delta_{\alpha\beta} + g' r r_\alpha r_\beta \quad (20)$$

Where  $r_\alpha = \frac{x_\alpha}{r}$ . Now this tensor is symmetric, with calculating  $u_{\alpha\beta}$  and  $\omega_{\alpha\beta} = 0$  putting it in (Eq. 17) above we get:

$$\frac{\partial Q_{\alpha\beta}}{\partial t} = \xi g' r \left( r_\alpha r_\beta - \frac{\delta_{\alpha\beta}}{2} \right) \quad (21)$$

With writing  $Q_{\alpha\beta}$  using :

$$Q_{\alpha\beta} = S \begin{bmatrix} \cos^2\theta - \frac{1}{2} & \sin\theta\cos\theta \\ \sin\theta\cos\theta & \sin^2\theta - \frac{1}{2} \end{bmatrix} \quad (22)$$

$$= \frac{S}{2} \begin{bmatrix} \cos(2\theta) & \sin(2\theta) \\ \sin(2\theta) & -\cos(2\theta) \end{bmatrix} \quad (23)$$

In polar coordinates  $(r, \phi)$  right hand side of (Eq. 21) is:

$$\frac{\partial Q}{\partial t} = \frac{\xi g' r}{2} \begin{bmatrix} \cos(2\phi) & \sin(2\phi) \\ \sin(2\phi) & -\cos(2\phi) \end{bmatrix} \quad (24)$$

If we combine (Eq.23) and (Eq.24):

$$-S \sin(2\theta) \frac{d\theta}{dt} = \frac{\xi g' r}{2} \cos(2\phi) \quad (25)$$

$$S \cos(2\theta) \frac{d\theta}{dt} = \frac{\xi g' r}{2} \sin(2\phi) \quad (26)$$

Multiply first equation (Eq.25) by  $-\sin(2\phi)$  and second equation (Eq.26) by  $\cos(2\phi)$  and sum them up:

$$\frac{d\theta}{dt} = \frac{\xi g' r}{2S} [\sin(2\phi)\cos(2\theta) - \cos(2\phi)\sin(2\theta)] \quad (27)$$

$$\frac{d\theta}{dt} = \frac{\xi g' r}{2S} \sin(2(\phi - \theta)) \quad (28)$$

Thus if  $g' > 0$ , equation above has a stable equilibrium for  $\theta = \phi$  (aster).

### **Data Availability**

All data supporting the findings in this study are available from the corresponding authors on request.

### **Code Availability**

All custom codes used in this study are available from the corresponding authors on request.

### **Acknowledgments**

This work was supported by an EMBO installation Grant (IG 3275, A.K.) and BAGEP young investigator award (A.K.). We thank Sharad Ramanathan for suggestions about bacterial competitions. We thank Julia Yeomans for discussions and suggestions. We thank F. M. Ramazanoğlu, A. Kabakçioğlu, and M. Muradoğlu for critical reading of the manuscript.

## Author contributions

M.B, Y.I.Y. and A.K. designed and performed experiments, analyzed data and developed the imaging systems. R.V. designed and developed the FEM simulation toolbox and optimized the codes with realistic bacterial parameters. M.B. continuum simulation algorithms and performed all the simulations. T.C.Y developed the image processing codes to analyze inward growing monolayer colonies. MB. and A.K. prepared the draft, and all authors contributed to the final writing of the manuscript.

## Competing interests

Authors declare no competing interests.

## Tables

Strain	Parent	Operation	Genotype
BAK47	168	Transformed with plasmid ECE321 from Bacillus Genetic Stock Center	<i>amyE::Pveg-sfGFP</i> (Spc)
BAK115	TMN1138	Transformed with plasmid ECE327 from Bacillus Genetic Stock Center	<i>amyE::Pveg-mKate</i> (Spc) <i>sacA::P<sub>hag</sub>-mKate2L</i> (Kan) <i>hagA233V</i> (Phleo)
BAK51	TMN1138	Transformed with plasmid ECE321 from Bacillus Genetic Stock Center	<i>amyE::Pveg-sfGFP</i> (Spc) <i>sacA::P<sub>hag</sub>-mKate2L</i> (Kan) <i>hagA233V</i> (Phleo)
BAK 55	DH5alpha	Transformed with plasmid 107741 from Addgene	<i>pDawn-sfGFP</i>

Table 1: List of strains used in this study.

## References

1. Grant, M.A.A., et al., *The role of mechanical forces in the planar-to-bulk transition in growing Escherichia coli microcolonies*. Journal of the Royal Society Interface, 2014. **11**(97).
2. Su, P.T., et al., *Bacterial Colony from Two-Dimensional Division to Three-Dimensional Development*. Plos One, 2012. **7**(11).
3. Volfson, D., et al., *Biomechanical ordering of dense cell populations*. Proceedings of the National Academy of Sciences of the United States of America, 2008. **105**(40): p. 15346-15351.
4. Warren, M.R., et al., *Spatiotemporal establishment of dense bacterial colonies growing on hard agar*. Elife, 2019. **8**.
5. Cho, H.J., et al., *Self-organization in high-density bacterial colonies: Efficient crowd control*. Plos Biology, 2007. **5**(11): p. 2614-2623.



6. Smith, W.P.J., et al., *Cell morphology drives spatial patterning in microbial communities*. Proceedings of the National Academy of Sciences of the United States of America, 2017. **114**(3): p. E280-E286.
7. Doostmohammadi, A., S.P. Thampi, and J.M. Yeomans, *Defect-Mediated Morphologies in Growing Cell Colonies*. Physical Review Letters, 2016. **117**(4).
8. Dell'Arciprete, D., et al., *A growing bacterial colony in two dimensions as an active nematic*. Nature Communications, 2018. **9**.
9. Doostmohammadi, A., et al., *Active nematics*. Nature Communications, 2018. **9**.
10. You, Z.H., et al., *Geometry and Mechanics of Microdomains in Growing Bacterial Colonies*. Physical Review X, 2018. **8**(3).
11. You, Z.H., D.J.G. Pearce, and L. Giomi, *Confinement-induced self-organization in growing bacterial colonies*. Science Advances, 2021. **7**(4).
12. Farrell, F.D.C., et al., *Mechanically Driven Growth of Quasi-Two-Dimensional Microbial Colonies*. Physical Review Letters, 2013. **111**(16).
13. Beroz, F., et al., *Verticalization of bacterial biofilms*. Nature Physics, 2018. **14**(9): p. 954-+.
14. Hartmann, R., et al., *Emergence of three-dimensional order and structure in growing biofilms*. Nature Physics, 2019. **15**(3): p. 251-+.
15. Yaman, Y.I., et al., *Emergence of active nematics in chaining bacterial biofilms*. Nature Communications, 2019. **10**.
16. Saw, T.B., et al., *Topological defects in epithelia govern cell death and extrusion*. Nature, 2017. **544**(7649): p. 212-+.
17. Copenhagen, K., et al. *Topological defects induce layer formation in Myxococcus xanthus colonies*. 2020. arXiv:2001.03804.
18. Shankar, S. and M.C. Marchetti, *Hydrodynamics of Active Defects: From Order to Chaos to Defect Ordering*. Physical Review X, 2019. **9**(4).
19. DeCamp, S.J., et al., *Orientalional order of motile defects in active nematics*. Nature Materials, 2015. **14**(11): p. 1110-1115.
20. Giomi, L., et al., *Defect Annihilation and Proliferation in Active Nematics*. Physical Review Letters, 2013. **110**(22).
21. Maroudas-Sacks, Y., et al., *Topological defects in the nematic order of actin fibres as organization centres of Hydra morphogenesis*. Nature Physics, 2021. **17**(2): p. 251-+.
22. Meacock, O.J., et al., *Bacteria solve the problem of crowding by moving slowly (vol 17, pg 205, 2021)*. Nature Physics, 2021. **17**(3): p. 416-416.
23. Thijssen, K. and A. Doostmohammadi, *Binding self-propelled topological defects in active turbulence*. Physical Review Research, 2020. **2**(4).
24. Shankar, S., et al., *Defect Unbinding in Active Nematics*. Physical Review Letters, 2018. **121**(10).
25. Rivas, D.P., et al., *Driven topological transitions in active nematic films*. Soft Matter, 2020. **16**(40): p. 9331-9338.
26. Duclos, G., et al., *Topological defects in confined populations of spindle-shaped cells*. Nature Physics, 2017. **13**(1): p. 58-62.
27. Opathalage, A., et al., *Self-organized dynamics and the transition to turbulence of confined active nematics*. Proceedings of the National Academy of Sciences of the United States of America, 2019. **116**(11): p. 4788-4797.
28. Martinez-Prat, B., et al., *Selection mechanism at the onset of active turbulence*. Nature Physics, 2019. **15**(4): p. 362-+.
29. Basan, M., et al., *Alignment of cellular motility forces with tissue flow as a mechanism for efficient wound healing*. Proceedings of the National Academy of Sciences of the United States of America, 2013. **110**(7): p. 2452-2459.
30. Lee, B., et al., *Local alignment vectors reveal cancer cell-induced ECM fiber remodeling dynamics*. Scientific Reports, 2017. **7**.
31. Vader, D., et al., *Strain-Induced Alignment in Collagen Gels*. Plos One, 2009. **4**(6).
32. Than-Trong, E. and L. Bally-Cuif, *Radial glia and neural progenitors in the adult zebrafish central nervous system*. Glia, 2015. **63**(8): p. 1406-1428.
33. Azizi, A., et al., *Nuclear crowding and nonlinear diffusion during interkinetic nuclear migration in the zebrafish retina*. Elife, 2020. **9**.
34. Jang, S.S., et al., *Specification and Simulation of Synthetic Multicelled Behaviors*. Acs Synthetic Biology, 2012. **1**(8): p. 365-374.
35. Giomi, L., et al., *Banding, excitability and chaos in active nematic suspensions*. Nonlinearity, 2012. **25**(8): p. 2245-2269.
36. Olmsted, P.D. and P.M. Goldbart, *Isotropic-Nematic Transition in Shear-Flow - State Selection, Coexistence, Phase-Transitions, and Critical-Behavior*. Physical Review A, 1992. **46**(8): p. 4966-4993.
37. Mishra, P. *Pattern Formation in Active Nematics*. 2017.
38. Atis, S., et al., *Microbial Range Expansions on Liquid Substrates*. Physical Review X, 2019. **9**(2).
39. Vetter, R., F.K. Wittel, and H.J. Herrmann, *Packing of elastic wires in flexible shells*. Epl, 2015. **112**(4).
40. Vetter, R., et al., *Finite element simulation of dense wire packings*. European Journal of Mechanics a-Solids, 2013. **37**: p. 160-171.

41. Duvernoy, M.C., et al., *Asymmetric adhesion of rod-shaped bacteria controls microcolony morphogenesis*. Nature Communications, 2018. **9**.
42. You, Z.H., et al., *Mono- to Multilayer Transition in Growing Bacterial Colonies*. Physical Review Letters, 2019. **123**(17).
43. Hallatschek, O., et al., *Genetic drift at expanding frontiers promotes gene segregation*. Proceedings of the National Academy of Sciences of the United States of America, 2007. **104**(50): p. 19926-19930.
44. Kayser, J., et al., *Emergence of evolutionary driving forces in pattern-forming microbial populations*. Philosophical Transactions of the Royal Society B-Biological Sciences, 2018. **373**(1747).
45. Farrell, F.D., et al., *Mechanical interactions in bacterial colonies and the surfing probability of beneficial mutations*. Journal of the Royal Society Interface, 2017. **14**(131).
46. Dion, M.F., et al., *Bacillus subtilis cell diameter is determined by the opposing actions of two distinct cell wall synthetic systems*. Nature Microbiology, 2019. **4**(8): p. 1294-1305.
47. Roostalu, J., et al., *Determinants of Polar versus Nematic Organization in Networks of Dynamic Microtubules and Mitotic Motors*. Cell, 2018. **175**(3): p. 796-+.
48. Ross, T.D., et al., *Controlling organization and forces in active matter through optically defined boundaries*. Nature, 2019. **572**(7768): p. 224-+.
49. Kruse, K., et al., *Asters, vortices, and rotating spirals in active gels of polar filaments*. Physical Review Letters, 2004. **92**(7).
50. Julicher, F., et al., *Active behavior of the cytoskeleton*. Physics Reports-Review Section of Physics Letters, 2007. **449**(1-3): p. 3-28.
51. Sokolov, A., et al., *Emergence of Radial Tree of Bend Stripes in Active Nematics*. Physical Review X, 2019. **9**(3).
52. Snezhko, A. and I.S. Aranson, *Magnetic manipulation of self-assembled colloidal asters*. Nature Materials, 2011. **10**(9): p. 698-703.
53. Yan, J., et al., *Vibrio cholerae biofilm growth program and architecture revealed by single-cell live imaging*. Proceedings of the National Academy of Sciences of the United States of America, 2016. **113**(36): p. E5337-E5343.
54. Davidovitch, B., et al., *Prototypical model for tensional wrinkling in thin sheets*. Proceedings of the National Academy of Sciences of the United States of America, 2011. **108**(45): p. 18227-18232.
55. Chowdhury, F., et al., *Defining Single Molecular Forces Required for Notch Activation Using Nano Yoyo*. Nano Letters, 2016. **16**(6): p. 3892-3897.
56. Prabhune, M., F. Rehfeldt, and C.F. Schmidt, *Molecular force sensors to measure stress in cells*. Journal of Physics D-Applied Physics, 2017. **50**(23).

## Figure Captions

**Figure 1. Experimental observation of inward growth of bacterial colonies and emergence of radial alignment.** **a)** Early stage of a closed area surrounded by growing bacterial colonies (*B. subtilis*). **b)** Snapshot of the radially aligned bacterial profile immediately before hole closure. **c)** A director field superimposed on an inward growing domain displaying radial alignment. Scale bar  $25\mu\text{m}$  **d)** The azimuthally averaged radial order parameter ( $S_R$ ) and velocity against the distance from the colony center for the colony snapshot given in (c). Error bars are defined as s.d. **e,g)** Simulation of 2D inward colony growth and regular expansion of bacterial colonies **f,h)** Schematic illustration of the velocity field (black arrow) and frictional force (red arrow) on bacteria in the inward and outward growing domain. Cell colors represent the radial order parameter ( $S_R$ ). Red represents radial alignment; blue, tangential alignment.

**Figure 1—video 1. Movie 2-** Radial alignment during inward growth and emergence of asters. The video shows the second example of a fluorescence image of GFP labeled *B. Subtilis* strain (BAK 51) during inward growth. The video is associated with Figure 1a-d. The duration of the experiment is 100 min and the scale bar is given in Figure 1a.

**Figure 1—video 2. Movie 4** 2D Simulation of the bacterial colony during regular expansion. The video is associated with Figure 1g.

**Figure 2. Numerical analysis of critical physical parameters during inward growth. a, b)** Plot of azimuthally averaged radial stress distribution ( $|\sigma_{rr}|$ ) at different time points of regular expanding and inward growing colonies against the distances from the center of the colony. Time points are given in cell division time ( $t$ ). **c,d)** Plot of the azimuthally averaged radial order parameter ( $S_R$ ) across the colonies. Radial order emerges not only below the critical radius but also beyond this level. Negative radial order corresponds to a tangential orientation or active anchoring. **e,f)** Comparison of azimuthally averaged radial velocity ( $v_r$ ) profiles of regular expanding and inward-growing colonies. Regular expanding colonies display a linear profile; however, inward growing colonies form a nonlinear velocity profile. Error bars are defined as s.d. and averaged over 25 simulations. **g)** Snapshots of gradual rotation of a single bacterium (green) into a radial orientation during inward growth. Similar bacterial rotation can be seen in experimental results (Figure 2—figure supplement 5).

**Figure 2—figure supplement 1** Plot of azimuthally averaged stress distribution ( $|\sigma_{\theta\theta}|$  and  $|\sigma_{r\theta}|$ ) at different time points of regular expanding and inward growing colonies against the distances from the center of the colony.

**Figure 2—figure supplement 2** Plot of azimuthally averaged Packing fraction of bacteria at different time points of regular expanding and inward growing colonies against the distances from the center of the colony.

**Figure 2—figure supplement 3** Molecular dynamics simulations of colony radius. **a)** Plot of the radius of the regular expanding colony against time. **b)** Plot of the inner and outer radius of the bacterial colony of the inward growing colony against time. Critical radius is determined by where  $v_r$  equals to zero. Critical radius shows constant profile immediately before hole closure.

**Figure 2—figure supplement 4** Experimental measurements of the velocity profile. **a)** Plot of the inner radius of inward growing bacterial domain against time. **b)** Plot of radial velocity ( $v_r$ ) of the inner edge of the inward growing bacterial domain in the experiment against time.

**Figure 2—figure supplement 5** Experimental images of gradual rotation of a single bacterium (labeled green) into a radial orientation during inward growth.

**Figure 2—figure supplement 6** Simulation results of growing bacterial colony and scalar order parameters ( $S$ ) under circular confinement defined by a fixed wall. Under both conditions, colonies can develop radial alignment.

*Figure 3. Continuum simulations of 2D colony growth. a,b) Scalar order parameter ( $S$ ) overlapped with the director field pattern of both regular expanding and inward-growing bacterial colonies. Comparison of azimuthally averaged c,d) radial order parameter ( $S_R$ ) and e,f) radial velocity ( $v_r$ ) profiles of the colonies against the distance from the center of the colony. In contrast with regular expanding colonies, inward-growing domains developed radial order throughout the colony. A sudden velocity drop near the edge of the colonies resulted in tangential orientation. Error bars are defined as s.d.*

**Figure 3—figure supplement 1** Continuum simulation results of colony density and velocity profiles. **a,b)** velocity field superimposed on a density profile of regular expanding and inward growing colony. **c,d)** Plot of azimuthally-averaged density against the distance from the colony center for regular expanding and inward growing colony

**Figure 3-video 1** Continuum simulation of 2D colony growth during regular expansion. The scalar order parameter is overlapped with the director field pattern. This video is associated with Figure 3a.

**Figure 3-video 2** Continuum simulation of 2D colony growth during regular expansion. Colony density is overlapped with velocity field pattern. This video is associated with Figure 3e.

**Figure 3—video 3** Continuum simulation of 2D colony growth during inward growth. Colony density is overlapped with velocity field pattern. This video is associated with Figure 3f .

*Figure 4. 3D colony growth and multi-layer formation. a,b) Snapshot of inward growing bacterial domains obtained through the finite element model simulation in 3D. The colors represent (a) the radial order parameter ( $S_R$ ) and (b) the vertical displacement of the bacteria during growth.  $L$  is the bacterial length. c) Experimental snapshot of the inward-growing domain indicating the transition between mono- to multi-layer.  $\Delta r$  represents the width of the monolayer bacteria domain.*

**Figure 4—figure supplement 1** Comparison of the formation of multi-layered colony structures with and without physical confinement. Using PDMS and glass flat surfaces as vertical confinement, cannot generate large bacterial monolayers. Bright white regions around the center correspond to the second and the third layers. Scale bar corresponds to 100  $\mu\text{m}$ .

**Figure 4—figure supplement 2** 3D FEM Simulation results of growing bacterial colony and radial order for a) freely expanding bacterial colony b) inward growing colony under spherical confinement. A confined colony can develop strong radial alignment. Gray surfaces were added for visualization purposes. Cell colors represent the radial order. The blue color on the surface indicates surface anchoring.

**Figure 5. Patterning initial distribution of growing bacterial colonies. a,b)** Snapshot of inward growing bacterial colonies on different surfaces. Initial bacterial distribution is defined by non-contact lithographic techniques with blue light exposure. Inward growing domains are formed by merging colonies originating from annulus-shaped initial distribution. **(a)** On an agarose surface, growing colonies easily form multi-layer structures and provide narrow monolayer inward growing domains. However, **(b)** on a low friction polycarbonate (PC) surface, bacteria form monolayer colonies and provide large-scale inward growing domains. Scale bar  $500\mu\text{m}$ . **c)** Magnified fluorescence image superimposed with director field of the inward growing domain indicating the radial alignment of bacteria.  $\Delta r$  represents the width of the monolayer region. Scale bar  $50\mu\text{m}$ . **d)** Radial order parameter ( $S_R$ ) and, **e)** Radial velocity profile ( $V_r$ ) as a function of distance across the monolayer colony. Velocity profile was extracted by using PIV algorithms around the center of the annulus shape (Figure 5-video 2). **f)** The experimentally measured inner and outer and critical radius. *d, e, f* are averaged over 4 four different colonies, starting from the same initial annulus-shaped distribution.

**Figure 5—figure supplement 1** Photomask with different annulus shapes was used to define the initial distribution of bacteria.

**Figure 5—figure supplement 2** Snapshot of inward growing bacterial domains with the color representing compressive stress (a) on individual bacteria, velocity profile (b), and azimuthally averaged  $|\sigma_{rr}|$  radial,  $|\sigma_{\theta\theta}|$  hoop stress, the velocity profile, and the positions of the first 5

extrusion events triggering the multi-layering process. (d-f) Snapshot of the colonies under different surface friction. Snapshots were taken during the first extrusion event before multilayer formation. The first verticalization processes are shown in red circles. (g) The width of the monolayer colony obtained through the finite element model simulation on flat surfaces as a function of friction coefficients.

**Figure 5—figure supplement 3** Sample SEM images of growing colonies on a PC membrane surface. Nutrition can leak from LB plate through the holes and provide a sufficient growth environment for bacteria.

**Figure 5—figure supplement 4** Fluorescence image of growing monolayer colony on a PC surface during inward growth. The bottom edge corresponds to the inner radius of the annulus shape. Large-scale radial alignment occurs around the colony. Scale bar 50  $\mu\text{m}$ .

**Figure 5—figure supplement 5** Sample fluorescence image of inward growing domain superimposed with director field showing large scale radial bacterial alignment. The bottom side corresponds to the inner leading edge of the colony. Scale bar 50  $\mu\text{m}$ .

**Figure 5—figure supplement 6** Fluorescence image of growing monolayer colony on a PC surface starting from a single bacterium. Scale bar 50  $\mu\text{m}$ .

**Figure 5—figure supplement 7** Sample PIV measurement used to determine the position of stationary regions indicating the critical radius  $R_c$ . Scale bar 20  $\mu\text{m}$ . The left side corresponds to the inward growing domain.

**Figure 5—figure supplement 8** Radial alignment of biofilm-forming bacteria during inward growth. a) Time evolution of growing chaining bacterial colonies starting from annulus-shaped initial geometry. b) Magnified fluorescence images indicating the radial alignment of the biofilm around the inner radius. The regions are highlighted in (a). c) FEM simulation of growing biofilm structure. d) Magnified images of simulation results indicating the radial alignment.

**Figure 5—video 1** Time evolution of growing colonies starting from annulus-shaped initial distribution. The initial bacterial pattern was defined by blue light exposure. The video shows the fluorescence image of GFP labeled *B. Subtilis* 1138 strain (BAK 51) during inward growth. This video is associated with Figure 5b. The scale bar is given in the Figure5b.



**Figure 5—video 2** High magnification timelapse imaging of bacterial growth around the critical radius.

**Figure 5—video 3** Time evolution of growing biofilm-forming colonies starting from annulus-shaped initial distribution. The initial bacterial pattern was defined by blue light exposure. The video shows the fluorescence image of GFP labeled biofilm-forming strain *B. Subtilis* 168 (BAK 47) during inward growth. This video is associated with **Figure 5—figure supplement 7**. The scale bar is given in the associated figure.

**Figure 5—video 4** 2D FEM simulation results of growing biofilm structure during inward growth. This video is associated with **Figure 5—figure supplement 7**.

**Figure 6. Simulations of bacterial competition during inward growth. a,b,c)** Plot of the azimuthally averaged radial order parameter ( $S_R$ ) for green and red species against the distance from the colony center. Division lengths of green and red species are (a)  $L_{red} = 4.5 \mu\text{m}$ ,  $L_{green} = 3 \mu\text{m}$  (b)  $L_{red} = 3 \mu\text{m}$ ,  $L_{green} = 3 \mu\text{m}$  (c)  $L_{red} = 3 \mu\text{m}$ ,  $L_{green} = 4.5 \mu\text{m}$  **d, e, f)** Snapshot of multispecies simulations immediately before hole closure (d)  $L_{red} = 4.5 \mu\text{m}$ ,  $L_{green} = 3 \mu\text{m}$  (e)  $L_{red} = 3 \mu\text{m}$ ,  $L_{green} = 3 \mu\text{m}$  (f)  $L_{red} = 3 \mu\text{m}$ ,  $L_{green} = 4.5 \mu\text{m}$ . (g) The plot of relative packing fraction  $((\Phi_{green} - \Phi_{red})/(\Phi_{green} + \Phi_{red}))$  as a function of distance from the center. (h) Simulation results of competing bacterial strains with equal and different division lengths immediately before hole closure. Long red bacteria form lanes and approach the center of the defect more efficiently. Error bars are defined as s.d.

**Figure 6- figure supplement 1** 2D simulation results of competing bacterial strains with different division lengths. Starting from random initial annulus distribution, the longest bacteria could develop higher radial order. This packed and random initial distribution is hypothetical to test the most the worst-case scenario to challenge bacterial competition.

**Figure 6- figure supplement 2** Experimental verification of bacterial segregation due to random fluctuation during inward growth. Competing RFP and GFP labeled, identical bacterial strains were mixed and printed on an agar surface using a sharp cylindrical object.

**Figure 6- figure supplement 3** Simulation results of competition of segregated bacterial strains. The longest bacteria can invade the center more effectively. After a complete invasion of the center, the radial lanes buckle.

### **Supplementary Video Captions:**

**Video 1- Movie 1-** Radial alignment during inward growth and emergence of asters. The video shows the fluorescence image of GFP labeled *E.coli* (BAK 55) during inward growth.

**Video 2-** 2D Simulation of a bacterial colony during inward growth. This video is associated with Figure 1f.

**Video 3-** Continuum simulation of 2D colony growth during inward growth. The scalar order parameter is overlapped with the director field pattern. This video is associated with Figure 3b.

**Video 4-** 3D FEM simulation of colony growth during inward growth. Color represents vertical displacement. This video is associated with Figure 4b.

**Video 5-** 3D FEM simulation of colony growth during inward growth. Color represents the radial order parameter. This video is associated with Figure 4a.

**Video 6-** 2D simulation results of competing bacterial strains with identical division lengths. RFP and GFP labeled bacteria are initially segregated. Color represents the bacterial type. This video is associated with Figure 6h.

**Video 7-** 2D simulation results of competing bacterial strains with different division lengths. RFP and GFP labeled bacteria are initially segregated. Color represents the bacterial type. This video is associated with Figure 6h.

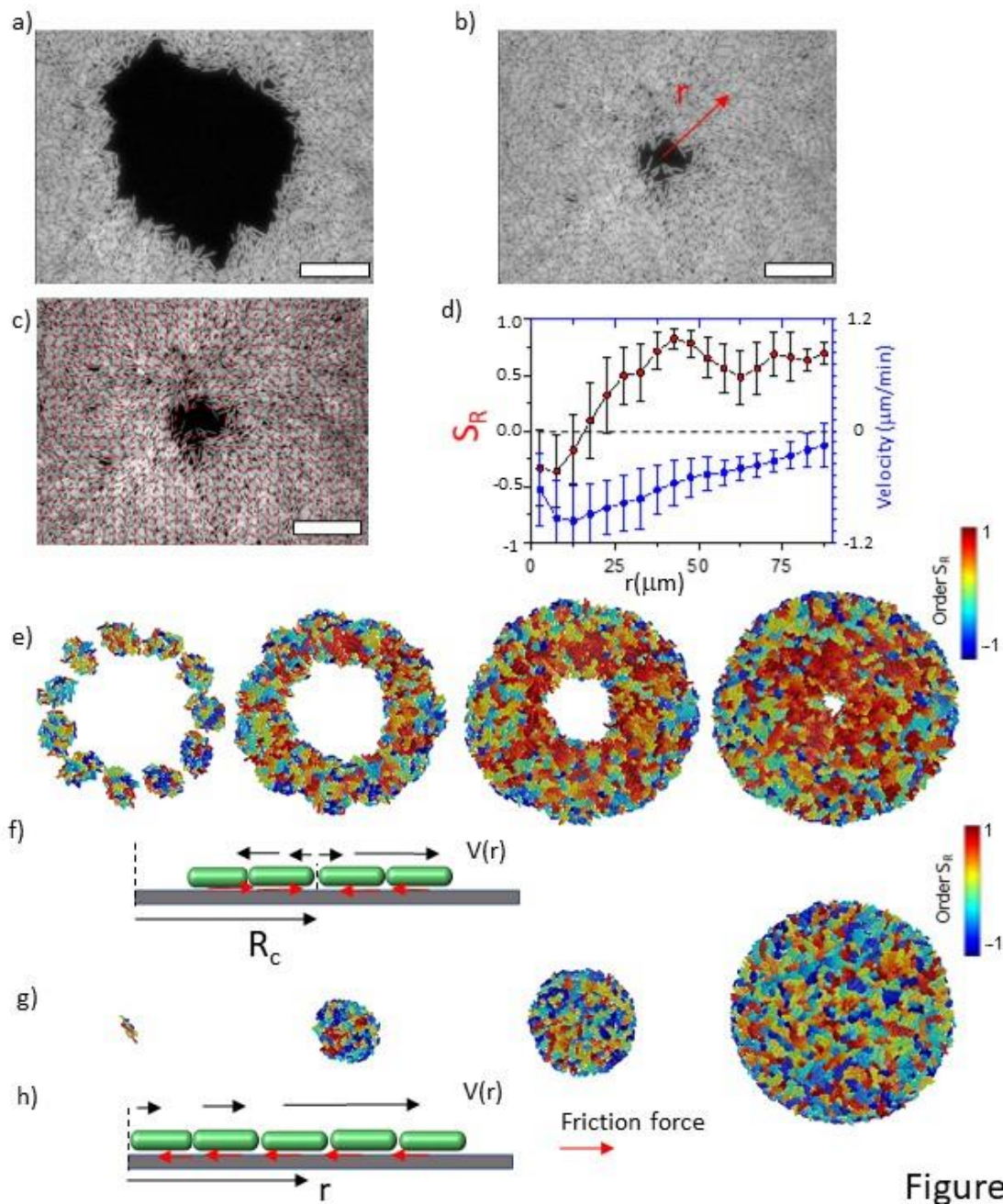


Figure 1

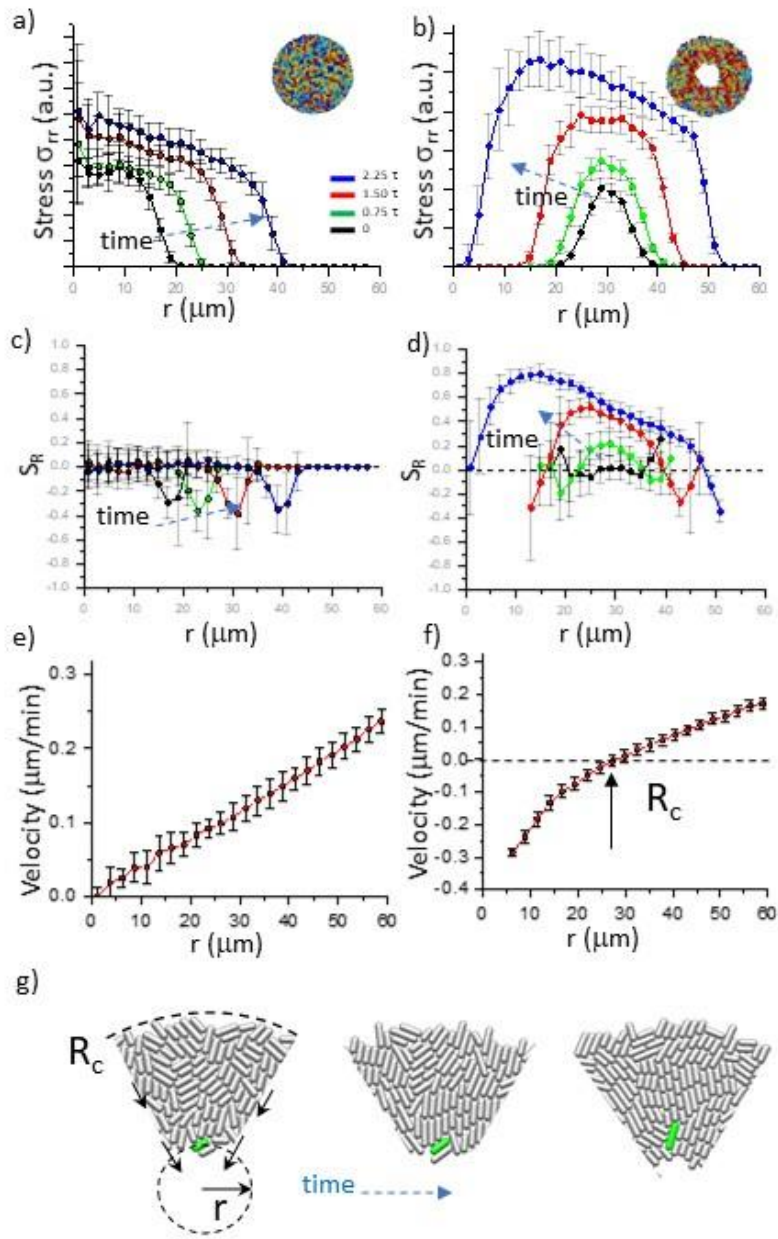


Figure 2

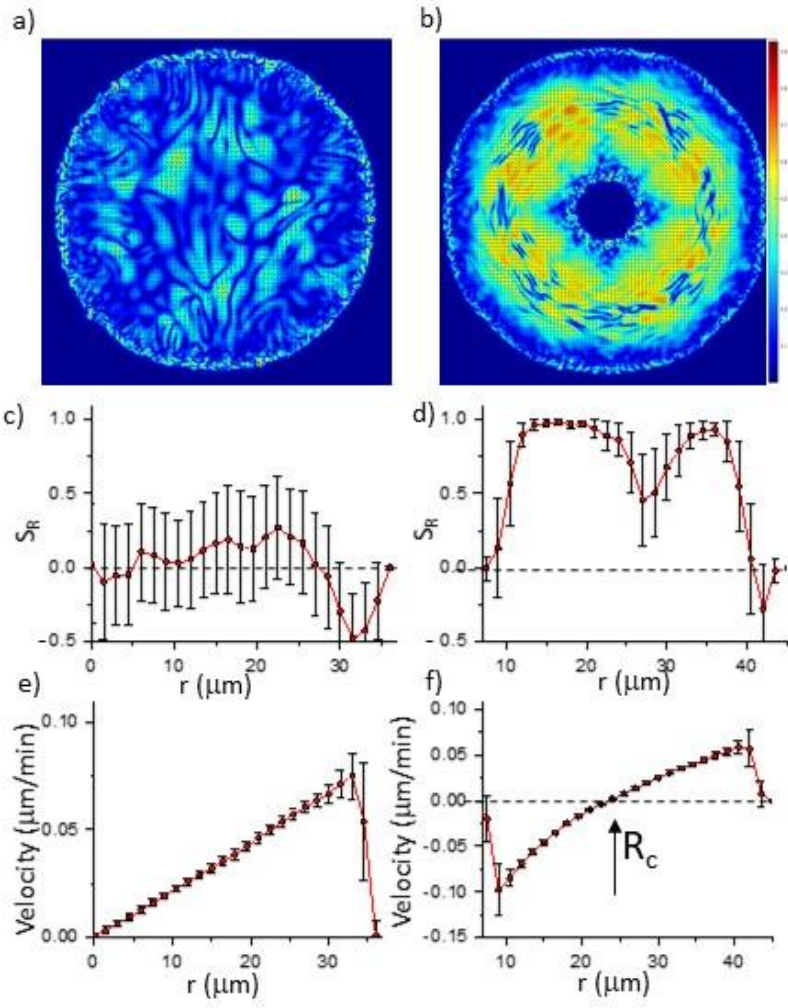


Figure 3

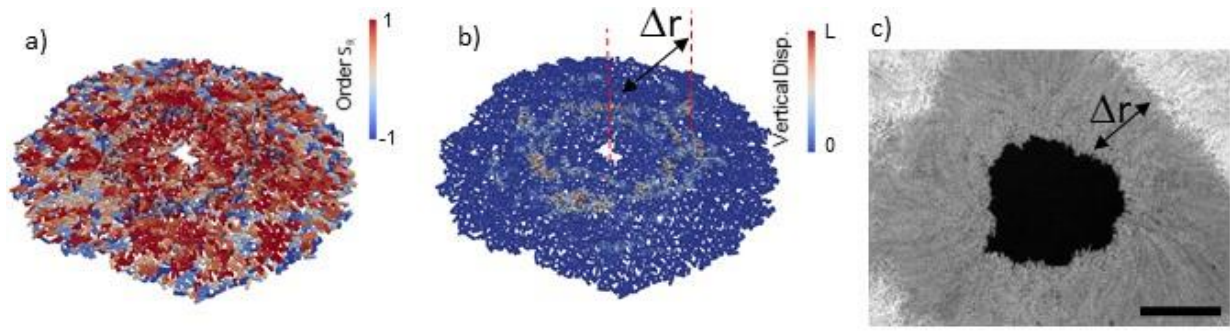


Figure 4



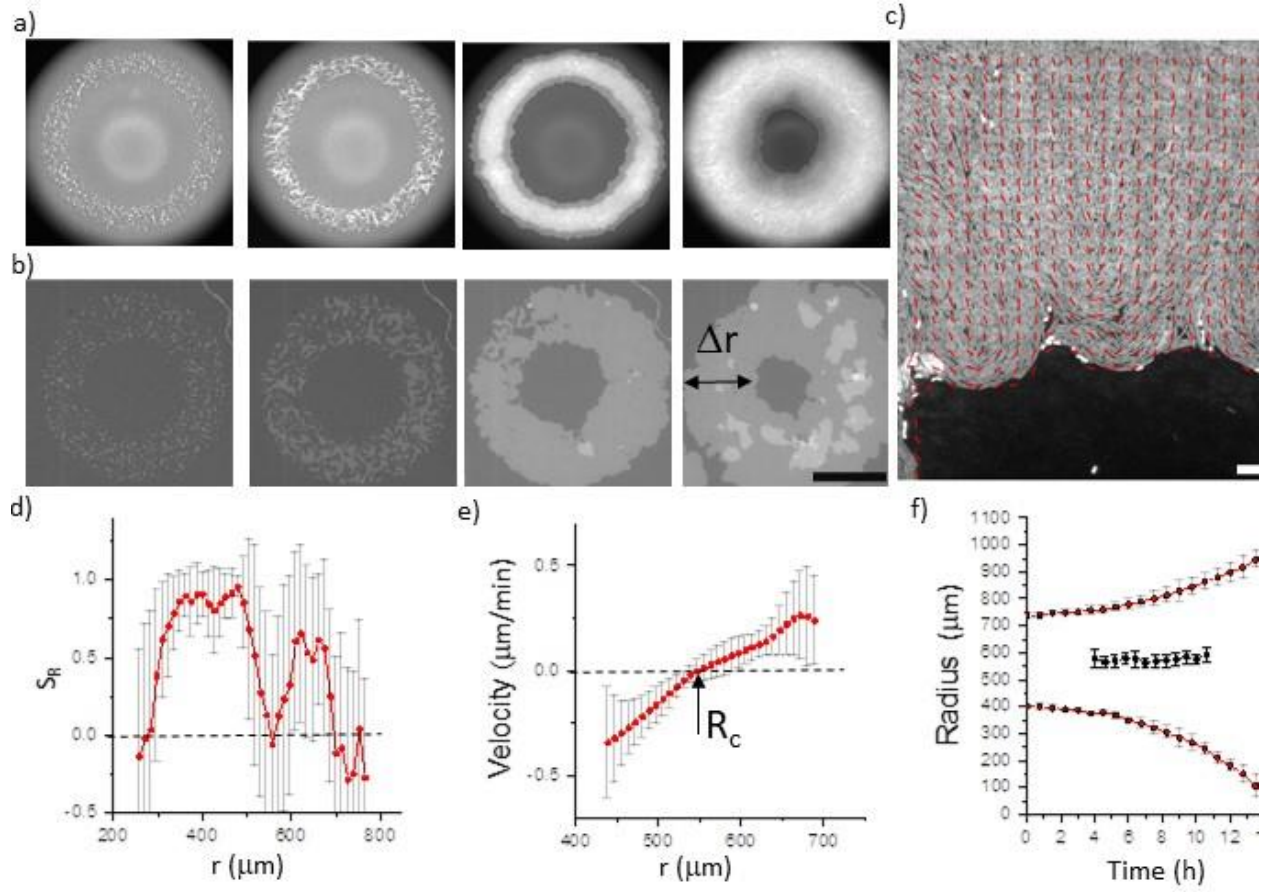


Figure 5

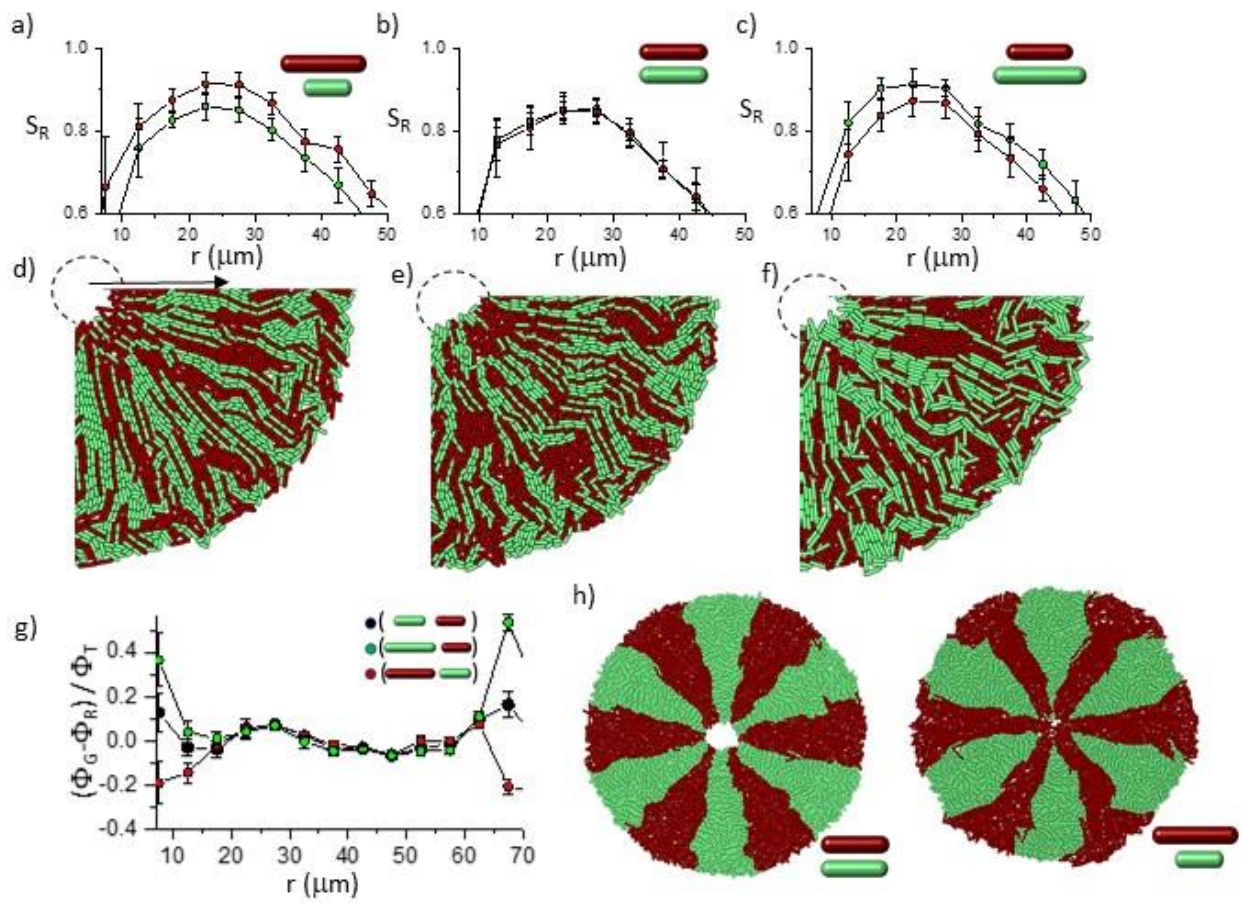


Figure 6



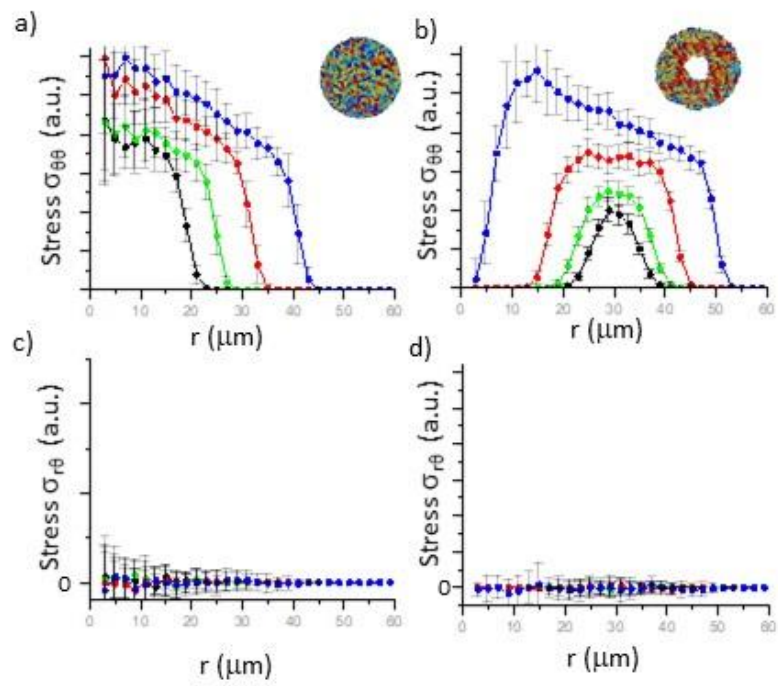


Figure2 - figure supplement 1

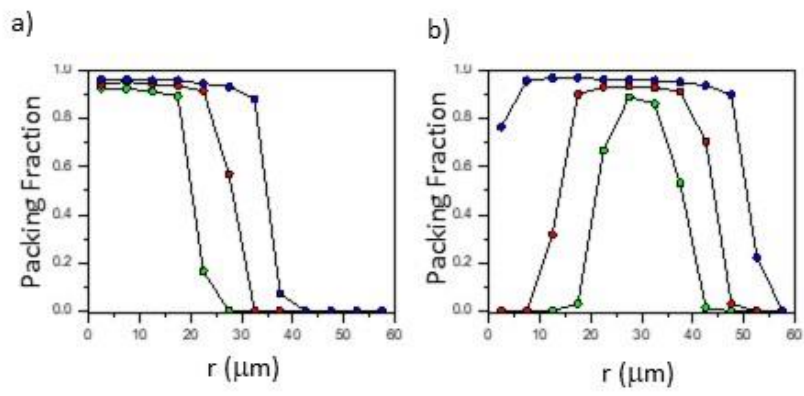


Figure2 - figure supplement 2

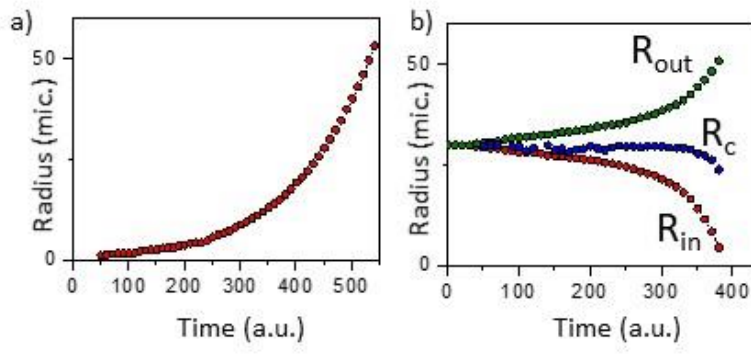


Figure2 - figure supplement 3

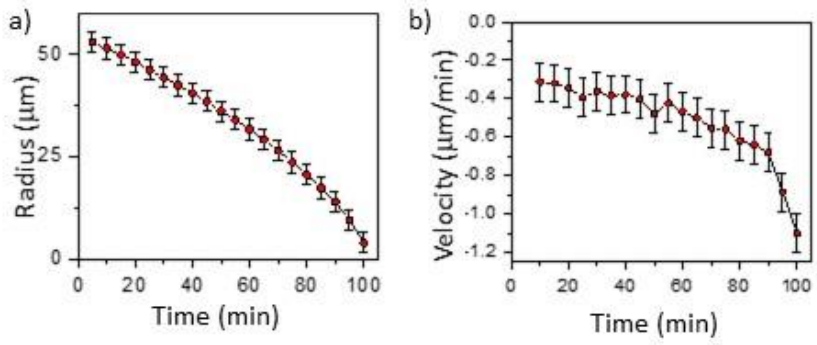


Figure2 - figure supplement 4

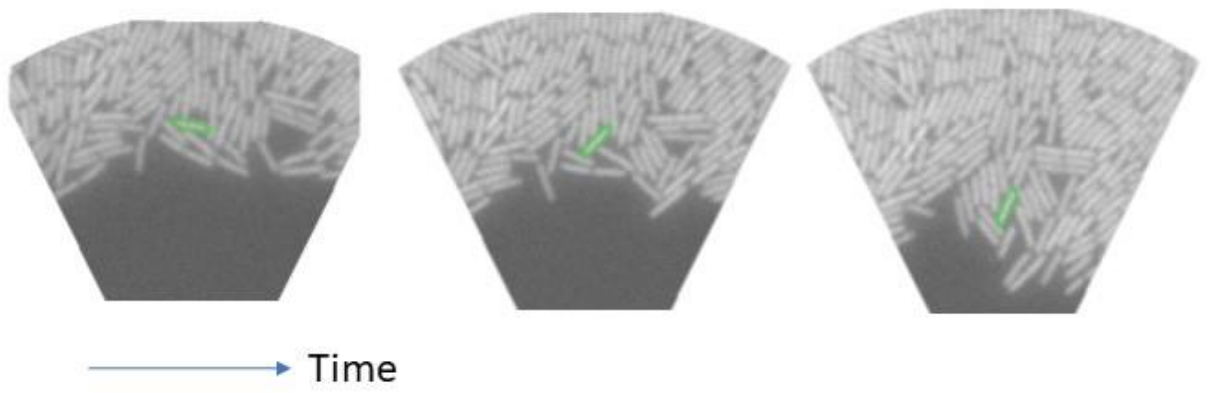


Figure2 - figure supplement 5

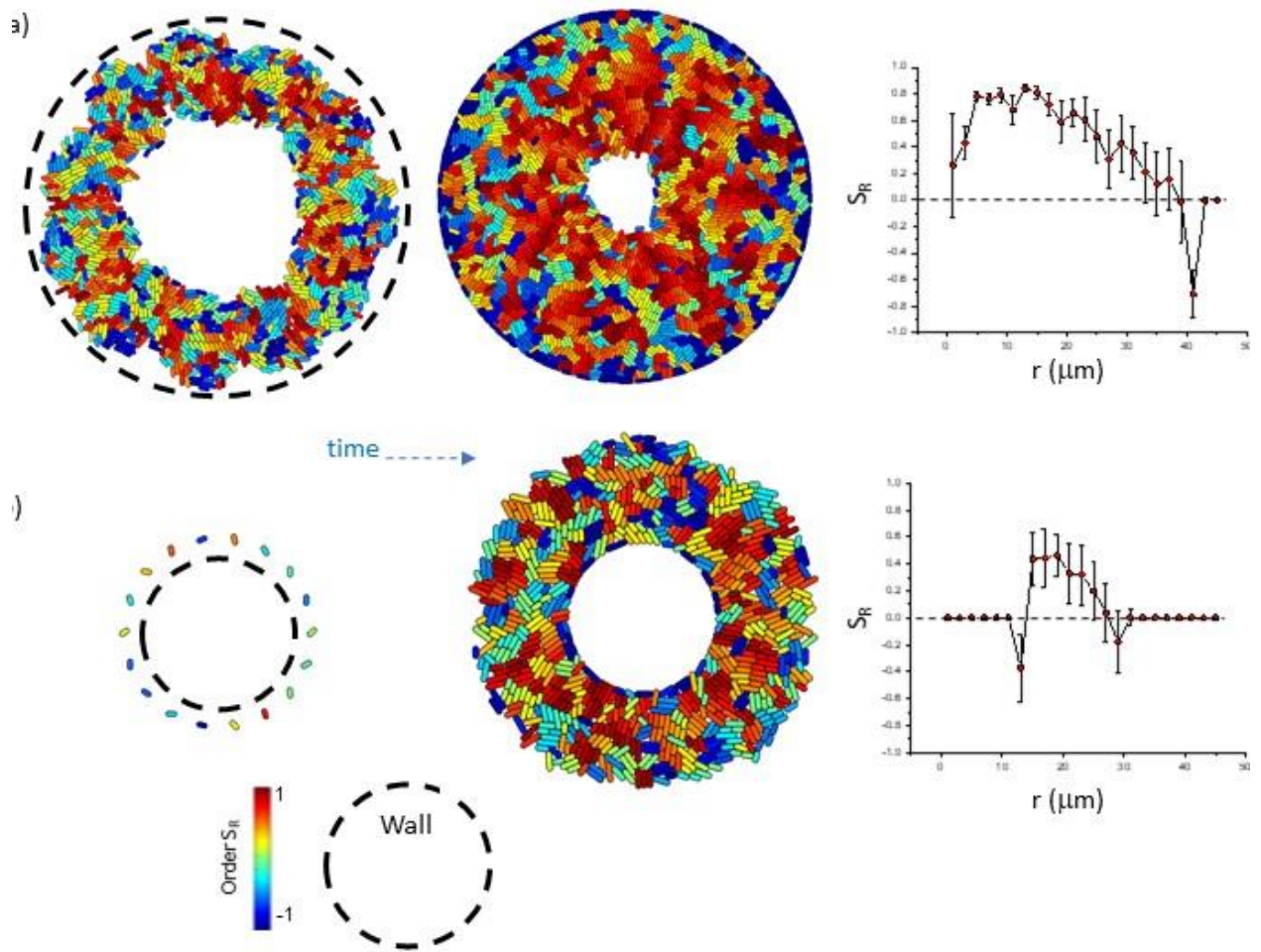


Figure2 - figure supplement 6

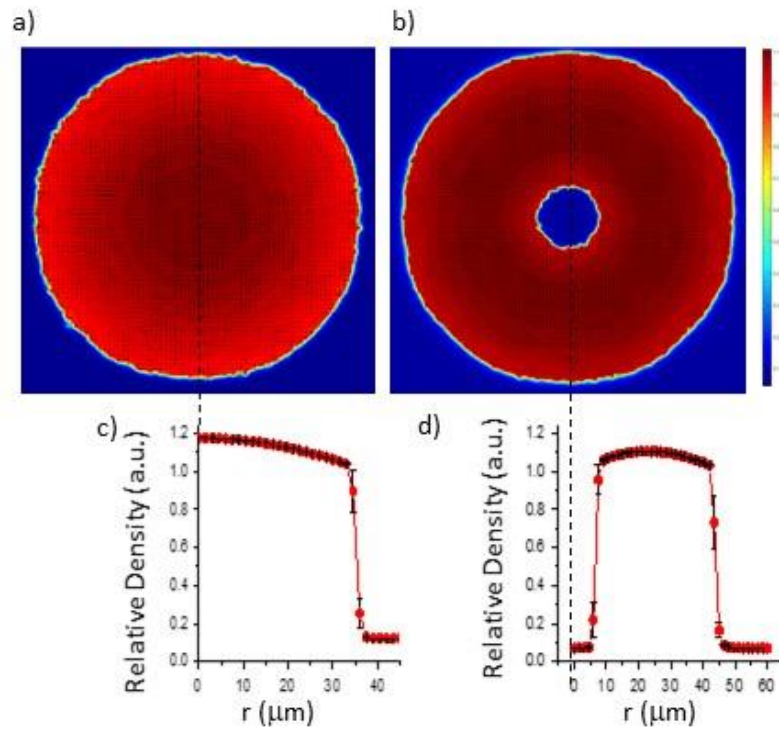


Figure 3- figure supplement 1

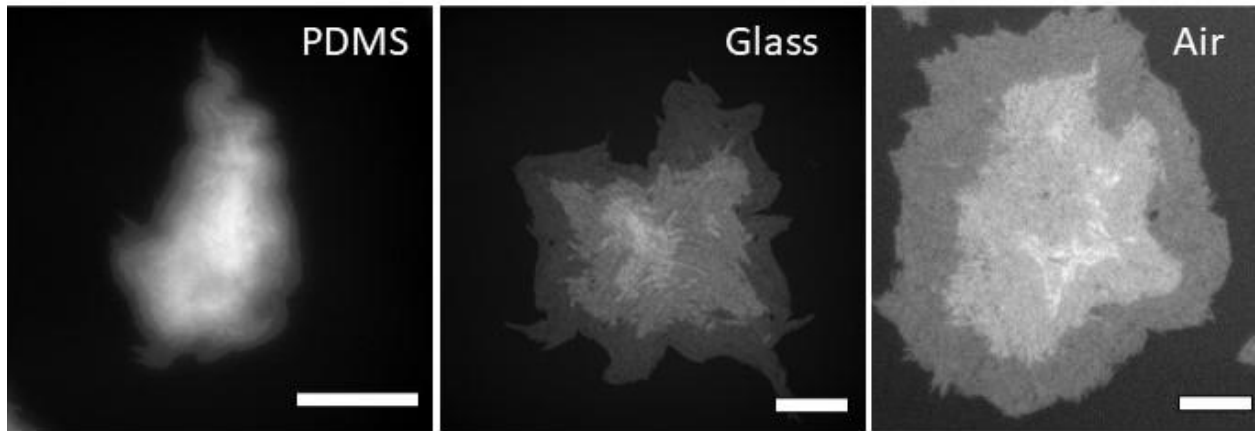


Figure 4- figure supplement 1



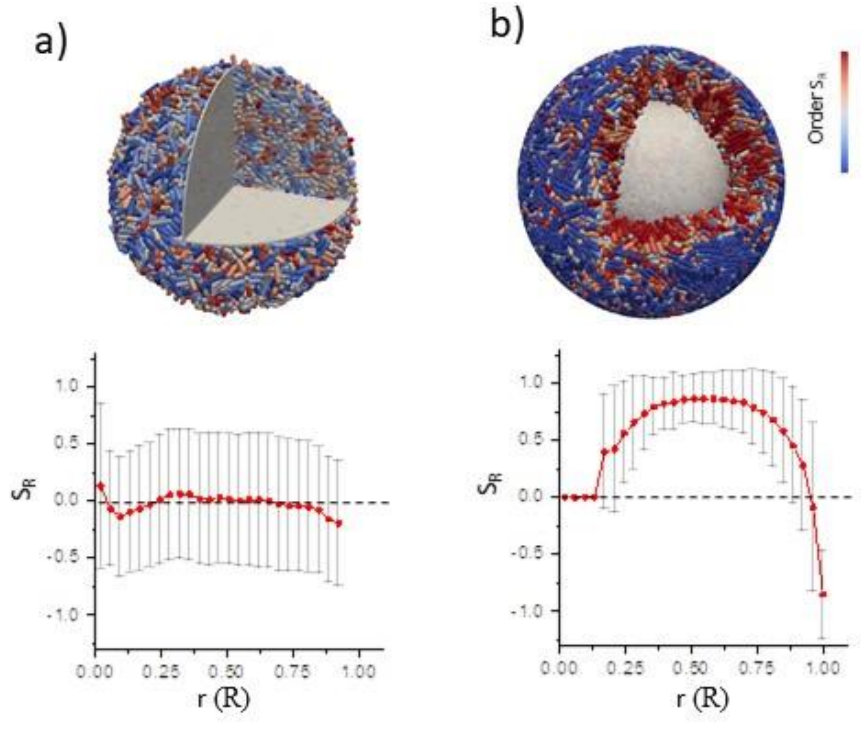


Figure 4- figure supplement 2

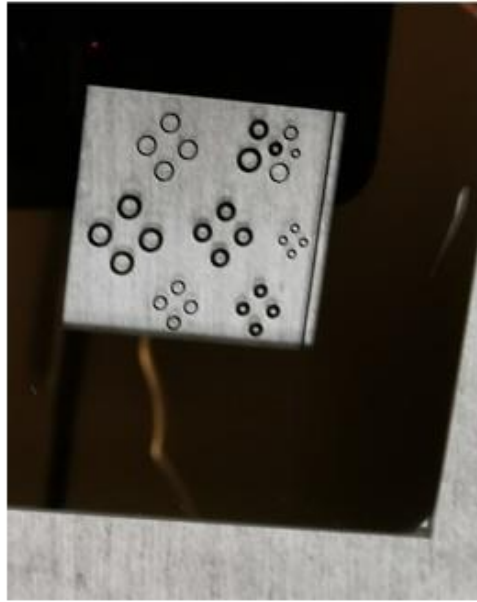


Figure 5- figure supplement 1

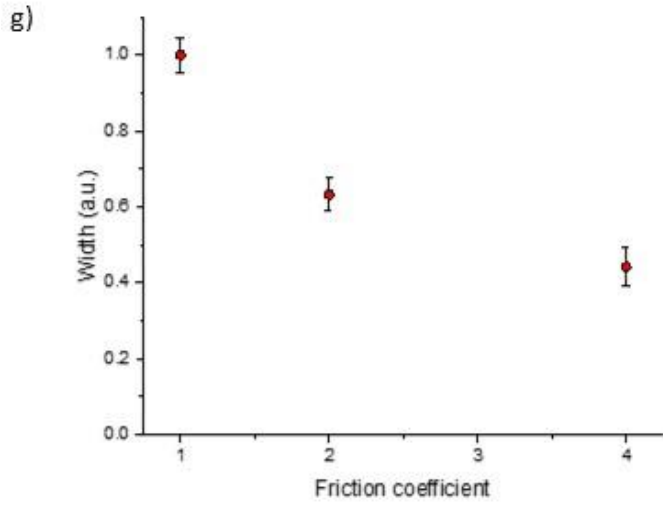
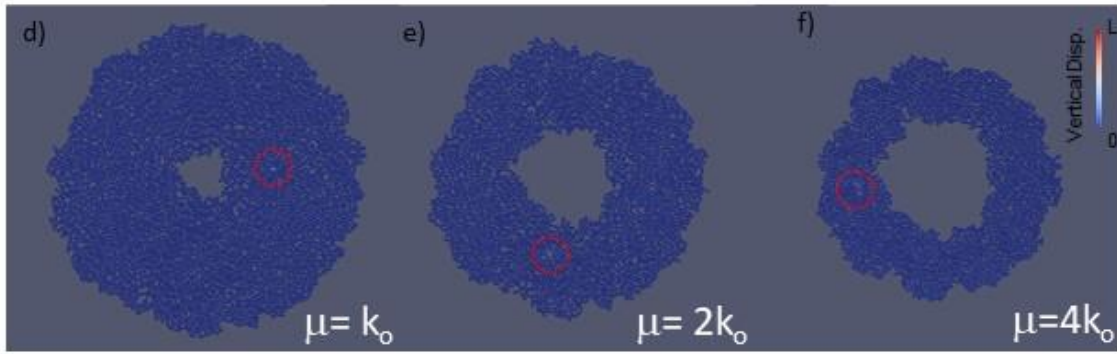
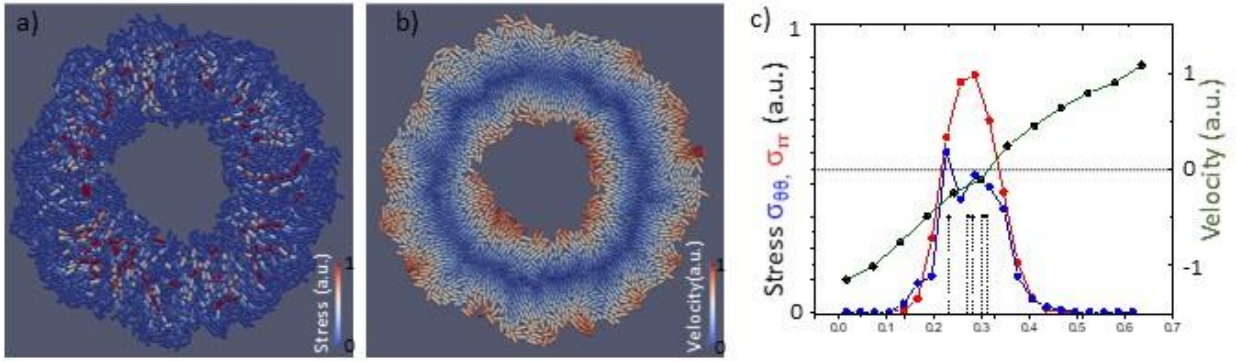


Figure 5- figure supplement 2

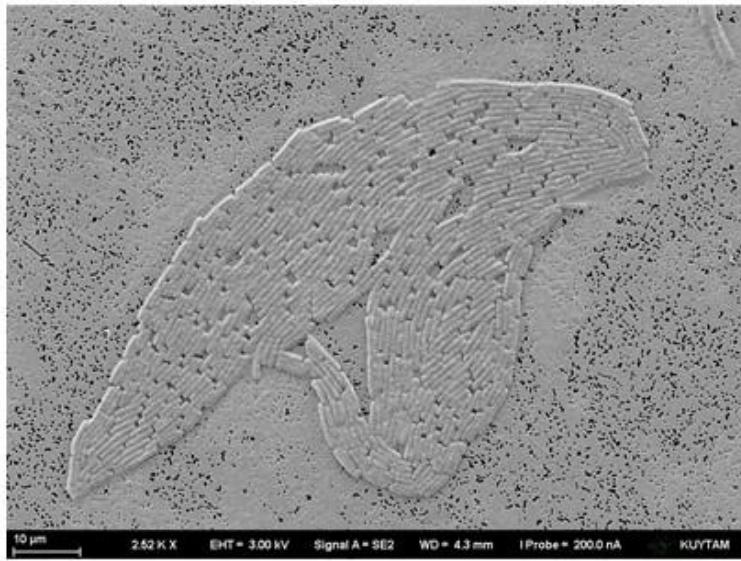
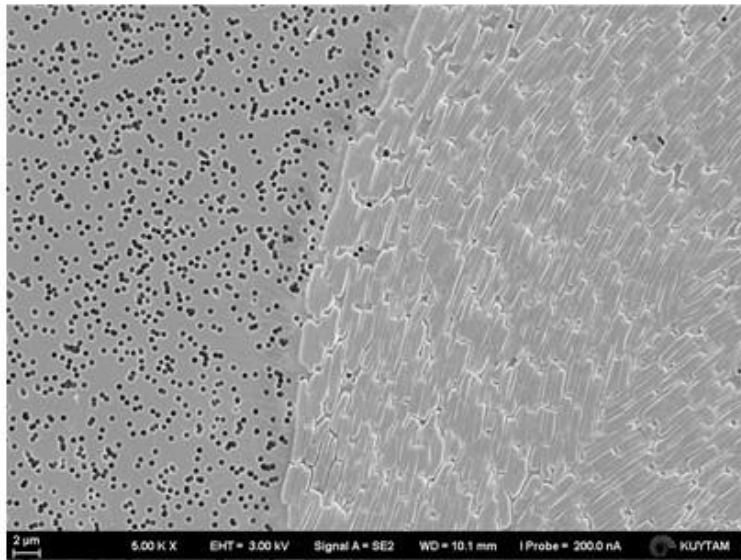


Figure 5- figure supplement 3



Figure 5- figure supplement 4

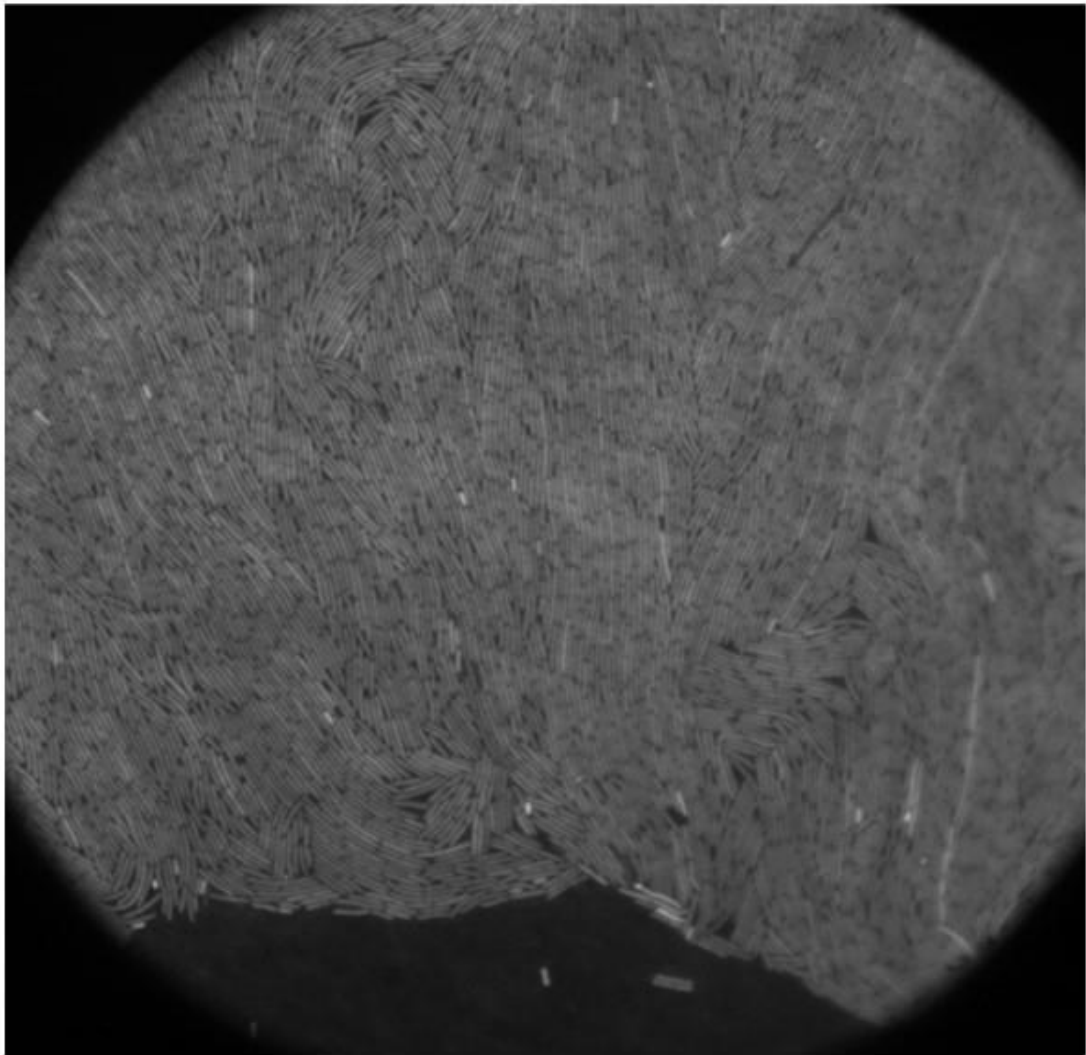


Figure 5- figure supplement 5

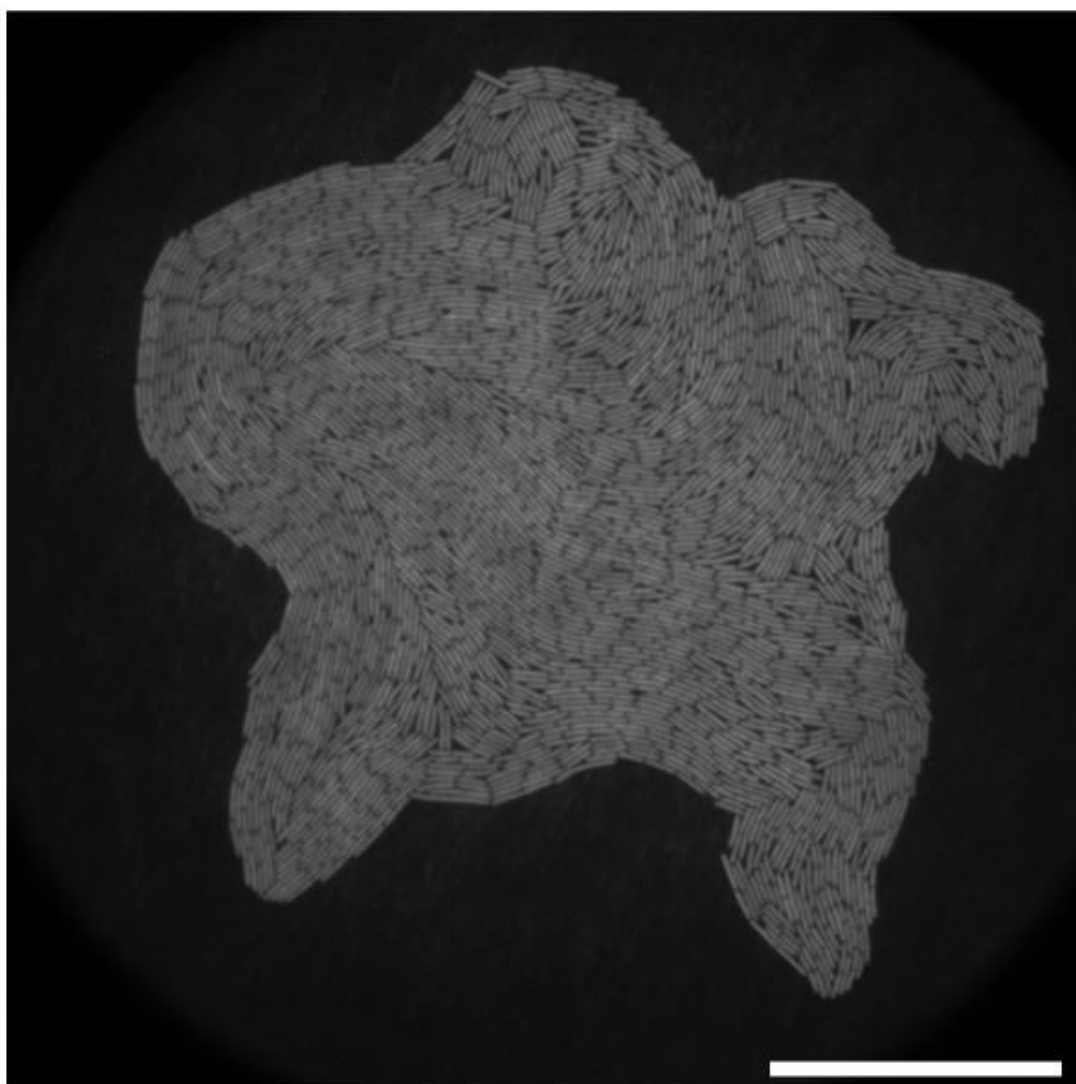
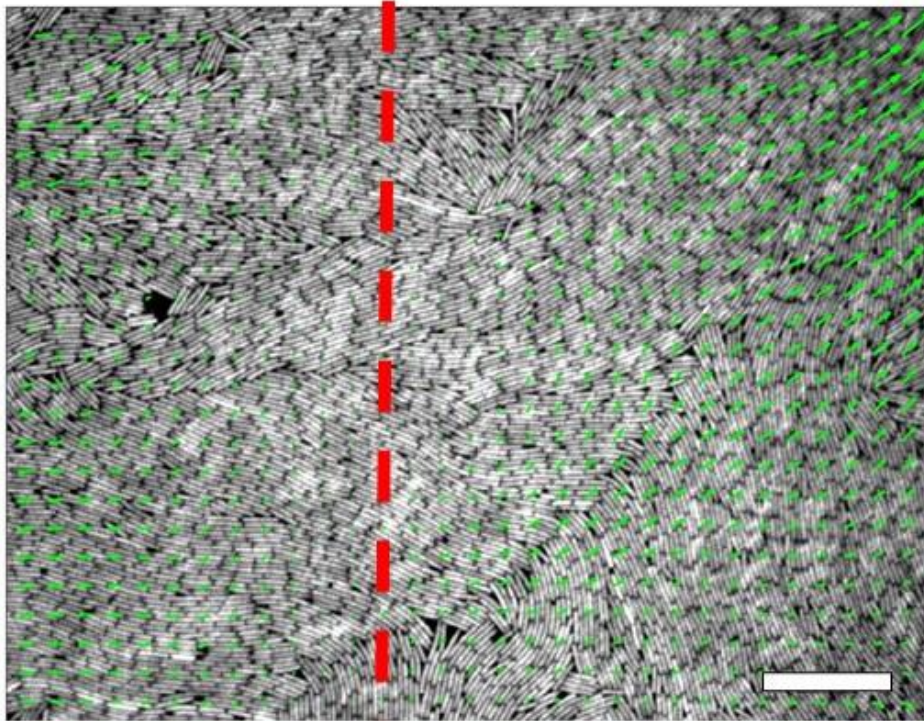


Figure 5- figure supplement 6





$R_c$

Figure 5- figure supplement 7



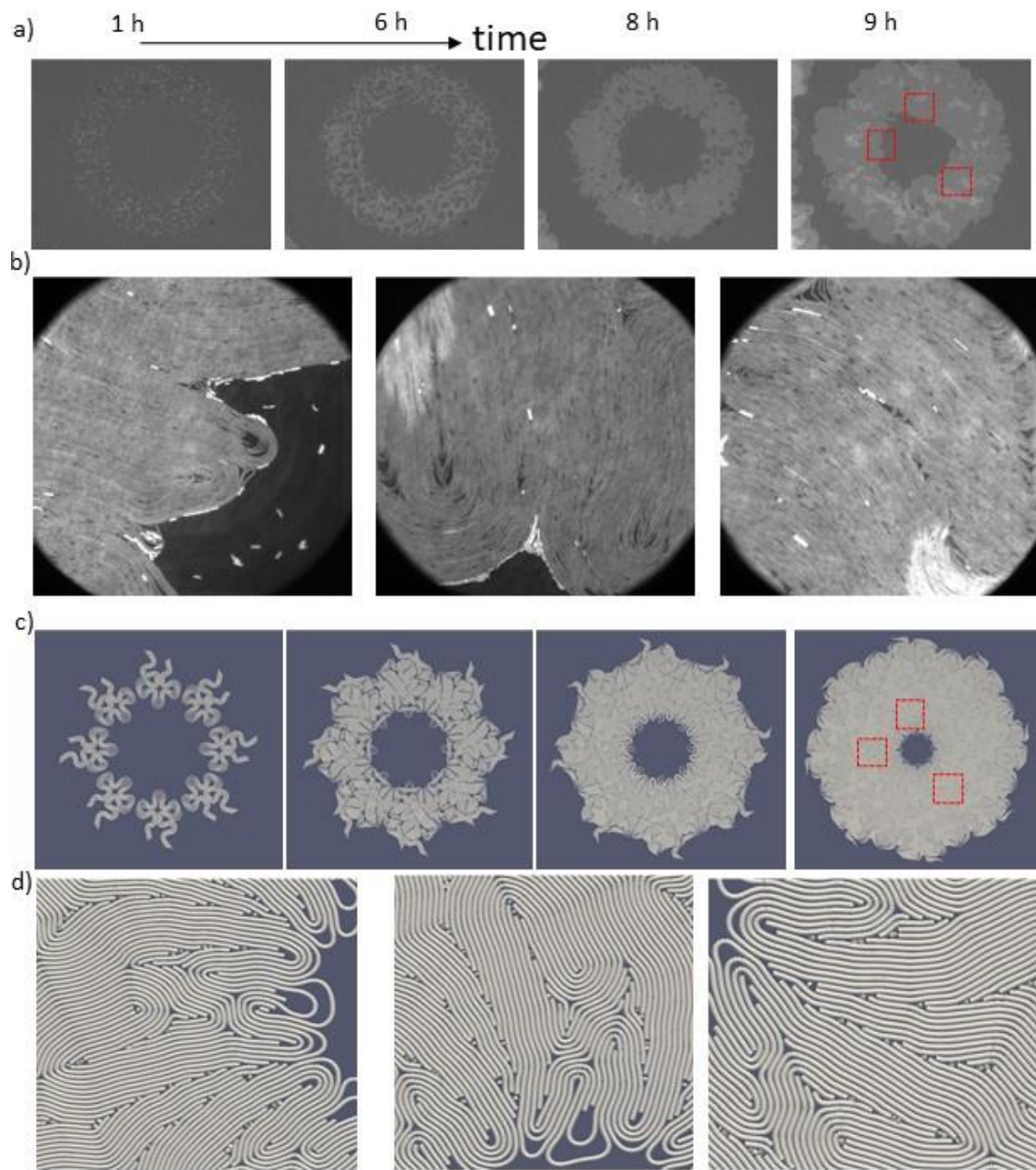


Figure 5- figure supplement 8

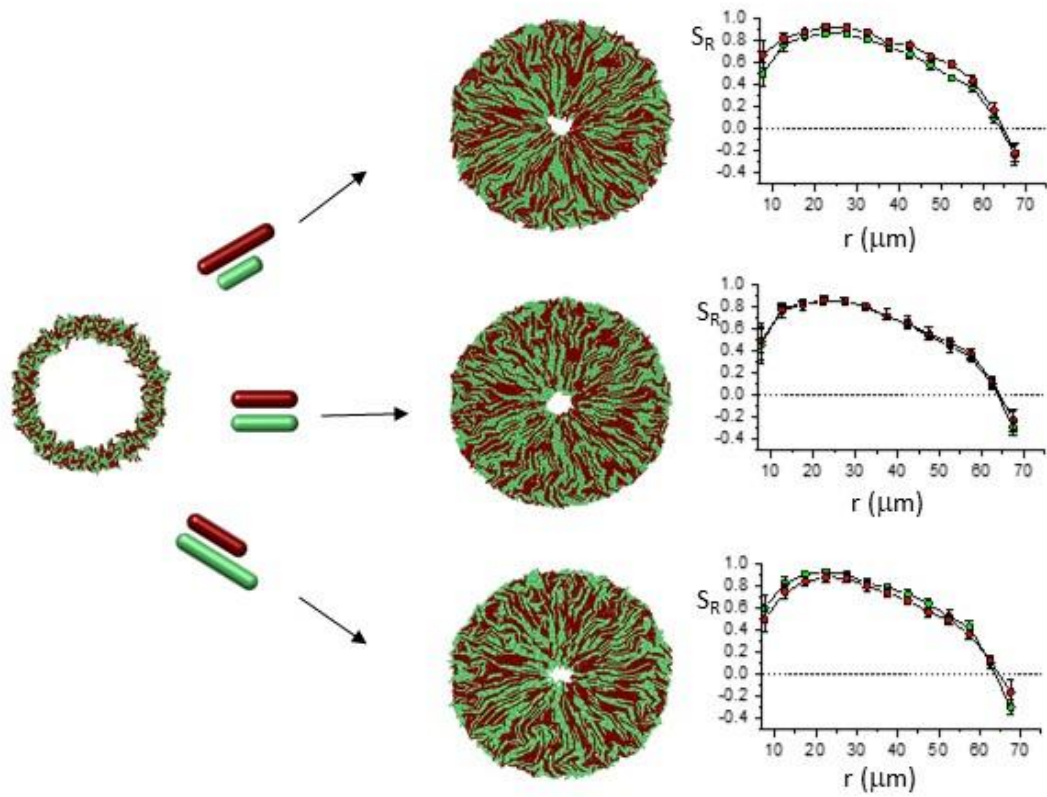


Figure 6- figure supplement 1

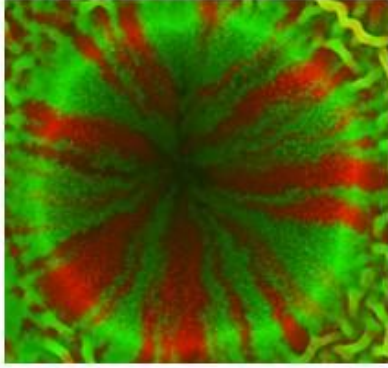
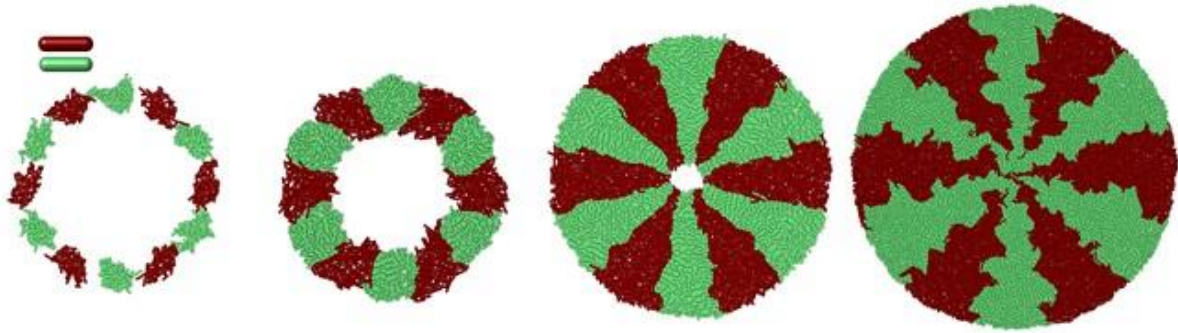


Figure 6- figure supplement 2

a)



b)

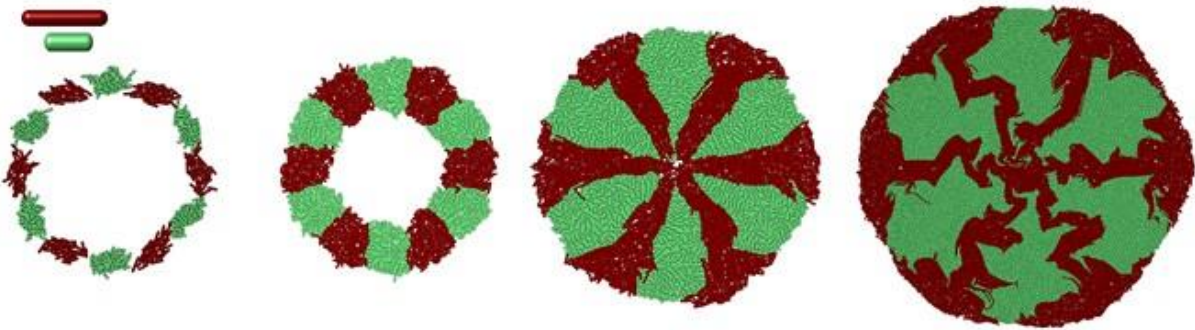


Figure 6- figure supplement 3

The Article was submitted to eLife and the public comments are given below:

Public Evaluation Summary:

The growth of bacterial colonies on solid substrates is a common assay used in a variety of settings, from probing bacterial organization in biofilms to spatial population genetics. The common setup is an outward growing colony from a central seed. In this work, Basaran et al., study a colony growing inward from an annulus. The authors show that this geometrical modification has profound consequences on the alignment of rod-shaped bacteria. This is caused by a flow alignment effect, and lead to a radial ordering reminiscent of an aster or +1 topological defect. This result is motivated by experimental observations with *E. coli* and interpreted using modern active matter theories, with ample support from extensive numerical simulations of detailed finite element and continuum models.

Reviewer #1 (Public Review):

This manuscript combines experiments, theory and simulation to study bacterial patterns in a colony growing inwards, from an annulus. The authors find that in this geometry growth leads to leads to the formation of an aster, which is a defect of topological charge +1, where bacteria tend to align in the radial direction. Previously, a growing colony of bacteria was reported to lead to nematic microdomain formation, with bacteria aligning tangentially at the colony edge, with half-integer defects in between microdomains. Overall I think this work is a nice example of an application of topology to bacterial biophysics, and is likely to appeal the growing active matter community.

The combination of experiments, theory and simulation renders the results convincing. It is nice that the theory allows to get a mechanistic and fundamental understanding of the reason for the aster formation, which can be traced back to the nonlinearity of the bacterial velocity/flow profiles. It is also nice that the simulations reproduce all previous observations in different geometries, providing validation of the current results.

Although overall the methodology is sound and the results appear robust, some clarifications are sought as follows.

1. In the orientational patterns in Fig. 3 it appears that some bacteria align out of the plane. If this is the case, and not a visualisation issue, it would be good to mention the relevance of the verticalisation, or to perform simulations where this is disallowed as in a growing monolayer.
2. It would be good to describe in a bit more detail how the plotted stress is computed in the simulation and how it could be estimated experimentally.
3. The patterns in multilayer colonies are of interest but it would be good to add a discussion of the reason why different surfaces lead to results which are so different.

Reviewer #2 (Public Review):

The growth of bacterial colonies on solid substrates is a common assay used in a variety of settings, from probing bacterial organization in biofilms to spatial population genetics. In this work, Basaran et al., study how crowded bacterial colonies invade an enclosed space, in contrast to the more common setup of a growing monolayer that expands outward in an unconstrained fashion. This seemingly innocuous modification has dramatic consequences as the authors show. Geometric confinement and growth from cell division dictate a characteristic velocity field that vanishes at a finite radius and the resulting shear flow aligns bacteria to orient in a radial fashion. The colony wide radial ordering is reminiscent of an aster or +1 topological defect seen in liquid crystals. A key point emphasized in the paper is that such large scale ordering of bacteria does not occur in outward expanding colonies, but is typical of inward growth. This result is motivated by experimental observations with *E. coli* and interpreted using modern active matter theories, with ample support from extensive numerical simulations of detailed finite element and continuum models. The structure and flow generated by radially oriented bacteria is shown to affect multilayering, both in simulations and in experiments with prepatterned annular rings of bacteria. Finally the authors demonstrate a potential biological significance of such orientational order by considering (in silico) two competing bacterial strains that are genetically neutral but have different lengths. The enhanced propensity of the longer bacterium to radially order endows it with a selective advantage to out compete the shorter strain in a spatial setting.

I find that most of the claims are well substantiated and justified by the data presented, though a few points need better support. The main strength of the paper is the involved and detailed numerical modelling employed to describe the invasion of bacterial colonies. It is an impressive amount of computational work. While some of the main points such as the emergence of a radial aster accompanied by a sign changing velocity field in inward growth are recapitulated in experimental data, the authors only make qualitative comparisons with the model. This I feel is a missed opportunity that can be easily remedied given the present data, particularly in the case of patterned colonies (Fig. 5). For instance, it is unclear what selects the critical radius  $R_c$ , and how it is determined by the initial inoculation geometry. A more quantitative comparison between the experimental and numerical data might help elucidate this point more.

Another weakness is in the discussion surrounding multilayer formation which is a bit disjointed and separate from the first part of the paper. The primary claim rests on a plausible argument suggesting compressive stresses near the critical radius cause buckling and multilayer formation, but the current data is only partially convincing. Fig. 4 only demonstrates the presence of multilayering in the finite element simulations and in the experiments but does not validate the suggested mechanism. A straightforward resolution would be to present measurements (at least from the simulation) of the hoop and radial stress in the monolayer and correlate it with the flow, radial order and buckling. The experimental demonstrations also lack descriptions of simple details regarding their setup at various places, which needs to be improved.

In the last section on bacterial competition with differential length strains, I feel the claim regarding the enhanced radial order in the longer bacterium is also not sufficiently substantiated. The red and green curves in Fig. 6a-f are meant to demonstrate this claim, but all three plots look rather similar and it is unclear how statistically significant the difference between the curves really is. Either the data must be presented along with a statistical analysis

demonstrating significant difference in radial order or the claim must be toned down. Note, the statement about enhanced radial order doesn't necessarily affect (though it is suggested as a causal mechanism) the more significant and consequential result regarding the excess area fraction of the longer bacterium over the shorter, which does demonstrate the claimed selective advantage.